PHYSICAL REVIEW B VOLUME 56, NUMBER 11 15 SEPTEMBER 1997-I

N-chain Hubbard model in weak coupling

Hsiu-Hau Lin
Department of Physics, University of California, Santa Barbara, California 93106

Leon Balents
Institute for Theoretical Physics, University of California, Santa Barbara, California 93106-4030

Matthew P. A. Fisher
Department of Physics, University of California, Santa Barbara, California 93106
and Institute for Theoretical Physics, University of California, Santa Barbara, California 93106-4030

(Received 6 March 1997)

We present a systematic weak-coupling renormalization group (RG) technique for studying a collection of N coupled one-dimensional interacting electron systems, focusing on the example of N-leg Hubbard ladders. For $N=2,3$, we recover previous results, and find that also more generally broad regions of the phase space of these models are unstable to pairing, usually with approximate d-wave symmetry. We show how these instabilities can be understood in terms of a fairly conventional ''gap'' function Δ at the discretized Fermi surface, and describe how this function is calculated. The dimensional crossovers as $N\rightarrow\infty$ and as many such ladders are weakly coupled together are also discussed. [S0163-1829(97)00836-9]

I. INTRODUCTION

Over the past few years, considerable interest has focused on systems of coupled chain conductors. Early theoretical studies of Heisenberg ladders (appropriate for the strongly interacting, nonitinerant half-filled limit) revealed an interesting odd/even effect.[1–5] If the number of legs of the ladder, N, is even, the system is expected to be a spin liquid with a singlet ground state and a (spin) gap to the lowest-lying excitations carrying angular momentum. For odd N, the ground state has quasi-long-range antiferromagnetic order and a set of gapless spin-wave excitations, which puts it in the universality class of the single spin-1/2 Heisenberg chain. Recent progress in the experimental preparation of relatively isolated spin ladders has begun to probe some of this rich physics and appears to have verified these expectations for $N=2,3$.[6–9] The behavior of *doped* ladders, i.e., those with itinerant charge carriers, is much richer. Particular theoretical attention has been paid to the case $N=2$, the two-leg ladder.[2,3,10–16] Early motivation stemmed from the possibility of realizing a concrete example of resonating valence bond ideas.[17,18] According to this line of thought, since the two-leg Heisenberg ladder is a spin liquid, the doped carriers experience a short-range attractive interaction, leading to pairing and the persistence of the spin gap. Such behavior is indeed observed in simulations of two-chain Hubbard[19–21] and t-J models,[2,22–25] which push the current computational limits of numerical methods working directly at zero temperature. Subsequent work by numerous authors has since demonstrated the existence of such a spin gap phase for low dopings by controlled analytical methods in weak coupling.[13,14,11] This weak-coupling approach has the additional advantage that it provides a full picture of the phase diagram, even away from half filling.

In this paper, we extend this analysis to more general N-chain Hubbard models.[26–29] Such an extension is useful in two respects. First, it allows a determination of the phase diagram for any small value of N, thereby elucidating the physics of doped spin liquids, the even/odd effect, and geometrical frustration. Furthermore, our equations allow a complete interpolation between one and two dimensions (along a particular path in parameter space—see below). An understanding of such a dimensional crossover[21] is a crucial first step in interpreting experiments in quasi-one-dimensional conductors.

To determine the behavior in the weak interaction limit, we employ a generalization of the renormalization group (RG) developed in Ref. 13 (the extension to the particular case $N=3$ has already by studied by Arrigoni[30,31]). This provides a systematic basis for treating the logarithmic divergences arising in a naive perturbative analysis. Coupled with the technique of bosonization, the primary output of the RG is a ''gap'' function Δ, describing pairing and the relative phase among the various spin and charge modes in the system. In the limit of large N, Δ becomes identical to the gap function defined in the conventional BCS theory of superconductivity, and one may thereby connect our results directly with higher dimensional analogs.

The RG also determines the zero temperature behavior as the chain length is taken to infinity. Because such a system is, for any finite N, still one-dimensional, it cannot sustain true off-diagonal long-range order, but is instead a generalized Luttinger liquid. The particular Luttinger liquid phase, within a general classification scheme developed in Ref. 13 also follows from the gap function Δ. We will use this notation, in which a phase with m gapless charge and n gapless spin modes is denoted $CmSn$, in what follows.

The results of our calculations for positive U Hubbard chains in the phase diagrams are summarized in Figs. 6–10. We emphasize that the phase diagrams are valid for arbitrary filling n and transverse hopping $t_\perp$ except at some specific lines (see below). First note the proliferation of phases as N

increases from 2 to 4. We believe that this complexity persists even in the $N\to\infty$ limit (but see below). The crossover to two dimensions is thus highly nontrivial. Second, despite the repulsive interactions, the majority of phases exhibit some degree of reduction of gapless spin modes, i.e., pairing. The symmetry of the pair wave function is in most cases consistent with a d-wave form. Unlike the two-chain case, however, as N is increased, gapless spin modes exist due to the presence of nodes in the pair wave function. Under different circumstances, as can be seen from Figs. 6–10, both $d_{x^2-y^2}$ and d_{xy} states appear.

A number of special results are obtained for particular small values of N. In the case $N=3$, the difference between open and periodic boundary conditions is quite pronounced, due to the strong role of frustration (and consequent absence of particle/hole symmetry) in the periodic case. As found previously by Arrigoni[30,31] and Schulz,[26] this Hubbard ''prism'' exhibits a spin gap at half filling, which persists over a range of both particle and hole doping. An especially surprising effect occurs for $N=4$ with periodic boundary conditions. In certain regions of the phase diagram, (singlet) Cooper pairs condense, not into the zero center-of-mass momentum state, but rather into the $m=\pm 2$ center-of-mass (quasi-)angular momentum states around the four-chain cylinder. We therefore call this a cylindrically extended (CEX) d-wave phase. Preliminary indications of the CEX d-wave phase have been found in recent numerical calculations.[32]

Although detailed phase diagrams such as these have only been obtained for $N=2,3,4$, our RG equations are valid for arbitrary N. They can be easily integrated numerically to any desired accuracy to determine most features of the weak-coupling phase diagram for any N. In the limit $N\to\infty$, several connections can be made with other work.[33] This limit may be taken in several ways. For the simplest form of our flow equations to remain valid, the interaction strength U must be scaled logarithmically to zero as $N\to\infty$. Strictly speaking, then, these RG equations do not describe truly two-dimensional systems with finite, nonsingular, interactions. The only logarithmic reduction of the domain of validity with increasing N suggests, however, that the two-dimensional limit may nevertheless be well approximated in this scheme. We present arguments that this is indeed the case. First, in the large N limit, our RG equations reduce, up to an overall normalization of the interaction strength, to those of Shankar,[33] derived directly in two dimensions. Second, an extended set of RG equations incorporating additional interactions, which we argue captures completely the two-dimensional limit for small nonzero U, can be shown to be equivalent to the previous ones for interactions with a nonsingular momentum dependence at the Fermi surface.

Based on these analyses, we expect our RG equations to contain a complete description of the dimensional crossover in the weak-interaction limit. In this limit, explicit analysis of the $1/N$ correction terms show that all the pairing instabilities occur only at very low temperatures, $T_c(N)\sim\Delta_N\sim e^{-N}$. Feedback of the forward-scattering interactions into the Cooper channel, responsible for the pairing instabilities in the smaller ladder systems at weak coupling, is therefore insufficient to produce superconductivity in the two-dimensional limit. We conclude that *strong* and/or nearly nested interactions are necessary to explain superconductivity in 2D repulsive Hubbard systems.

The remainder of the paper is organized as follows: In Sec. II, we introduce the N-chain Hubbard model, its weak-coupling limit, and a compact current-algebra notation for the allowed interactions. In Sec. III, the RG equations are derived using the operator product expansion to one loop order, and the numerical method used to study these equations is explained. In Sec. IV, we show how the results of these numerics can be understood using bosonization, introducing the gap function Δ in this context. These techniques are applied in Sec. V to determine the phase diagrams of three- and four-chain systems. Our analysis of the 2D limit is given in Sec. VI, and implications for numerics and experiments are discussed in Sec. VII. Four Appendixes give further details of current algebra methods, RG equations for umklapp couplings, initial values of coupling constants for the Hubbard models, and Klein factors needed for the bosonization calculations.

II. N-CHAIN HUBBARD MODEL

The N-chain Hubbard model is described by the Hamiltonian $H=H_0+H_U$,

$$H_0=\sum_{x,i,\alpha}\{-t[d^\dagger_{i\alpha}(x+1)d_{i\alpha}(x)+\text{H.c.}] - t_\perp[d^\dagger_{i+1\alpha}(x)d_{i\alpha}(x)+\text{H.c.}]\}, \tag{2.1}$$

$$H_U=\sum_{i,x}U{:}d^\dagger_{i\uparrow}(x)d_{i\uparrow}(x)d^\dagger_{i\downarrow}(x)d_{i\downarrow}(x){:}, \tag{2.2}$$

where $d_i(d_i^\dagger)$ is a fermion annihilation (creation) operator on chain i $(i=1...N)$, and $\alpha=\uparrow,\downarrow$ is a spin index. The parameters t and $t_\perp$ are hopping amplitudes along and between the chains, and U is an on-site Hubbard interaction.

We begin by diagonalizing the quadratic part of the Hamiltonian, H_0, as appropriate in the weak-coupling limit, $U\ll t,t_\perp$. This is accomplished by transforming to new fermion fields ψ_i, where

$$d_{j\alpha}=\sum_m S_{jm}\psi_{m\alpha}. \tag{2.3}$$

The transformation matrix S depends upon the boundary conditions in the transverse (y) direction. For periodic boundary conditions (PBC's), the eigenfunctions are plane waves, and

$$S_{jm}=\sqrt{\frac{1}{N}}\exp\left(\frac{2\pi i}{N}jm\right)\quad\text{(PBC)} \tag{2.4}$$

while for open boundary conditions (OBC's), the transverse eigenfunctions are standing waves,

$$S_{jm}=\sqrt{\frac{2}{N+1}}\sin\left(\frac{\pi}{N+1}jm\right)\quad\text{(OBC)}. \tag{2.5}$$

This brings the Hamiltonian into diagonal form in momentum space:

$$H_0=\sum_{i,\alpha}\int_{-\pi}^{\pi}\frac{dp}{2\pi}\epsilon_i(p)\psi_{i\alpha}^{\dagger}(p)\psi_{i\alpha}(p). \tag{2.6}$$

The single-particle energy is

$$\epsilon_i(p)=-2t\cos p-2t_{\perp}\cos(k_{yi}). \tag{2.7}$$

A difference in the spectra between OBC's and PBC's arises due to a difference in the set of allowed transverse momenta. These are

$$k_{yi}=\frac{\pi}{N+1}i,\quad i=1,2,\ldots,N \quad \text{for OBC's;} \tag{2.8}$$

$$k_{yi}=\frac{2\pi}{N}i,\quad i=0,\pm1,\ldots,(\pm)\left[\frac{N}{2}\right] \quad \text{for PBC's,} \tag{2.9}$$

where $[x]$ means the largest integer less than x. In the case of PBC, the momenta for $k_{yi}=\pm\pi$ are equivalent (i.e., differ by 2π) for N even. For this reason, we have enclosed the final $\pm$ in Eq. (2.9) in parentheses, which indicates that for N even, only one of these should be included for the proper counting of modes.

Equation (2.7) defines N bands, which, in weak coupling, are filled up to the chemical potential (Fermi energy) μ. For those bands which are partially filled, this defines a set of Fermi points $\{k_{Fi}\}$ via

$$\epsilon_i(k_{Fi})=\mu. \tag{2.10}$$

The chemical potential is fixed in terms of the physical density n (measured as a particle number per site) by the implicit condition

$$\sum_i k_{Fi}=\frac{\pi}{2}Nn\equiv Nk_F. \tag{2.11}$$

We now turn to the treatment of interactions. It is useful to introduce a functional integral formulation. Correlation functions are calculated as averages with respect to a ''Boltzmann weight'' e^{-S}, whose (Grassman) integral is the partition function (for example, see Ref. 34)

$$Z=\mathrm{Tr}e^{-\beta H}=\int[d\bar{\psi}][d\psi]e^{-S}, \tag{2.12}$$

where $\beta=(k_BT)^{-1}$ is the inverse temperature. Unless explicitly stated otherwise, all calculations in this paper are performed at zero temperature, i.e., $\beta=\infty$. The (imaginary time) action S is

$$S=\int_0^{\beta}d\tau\left[\sum_{i\alpha x}\bar{\psi}_{i\alpha}(x)\partial_{\tau}\psi_{i\alpha}(x)+H\right], \tag{2.13}$$

and $\bar{\psi}$ and ψ are Grassman fields.

In this formulation, it is straightforward to focus on the low-energy properties of the system. This is accomplished by integrating out all Grassman variables corresponding to fermionic operators creating excitations with substantial gaps. In particular, we first integrate out completely all $\psi_{i\alpha}$ and $\bar{\psi}_{i\alpha}$ corresponding to completely filled or empty bands, for which all excitations are separated by a finite energy from the chemical potential. When interactions are included, this gives rise to modifications of the remaining effective action of $O(U^2/t,U^2/t_{\perp})$, negligible relative to the bare $O(U)$ couplings for $U\ll t$. We denote the number of remaining partially filled bands by $N_f\leqslant N$. Second, we also integrate most of the longitudinal momentum modes in the partially filled bands, leaving only those in a width 2Λ around each Fermi point k_{Fi} (we will return to fix Λ later). That is, we integrate out $\psi_{i\alpha}(p)$ and $\bar{\psi}_{i\alpha}(p)$, provided $|p-k_{Fi}|>\Lambda$ *and* $|p+k_{Fi}|>\Lambda$. This again leads to a renormalization of the ''bare'' couplings in the remaining effective action, this time with the additional logarithmic factor

$$U_R\simeq U\left[1+\text{const}\times\frac{U}{t}\ln(k_F/\Lambda)\right]. \tag{2.14}$$

This second step of integration is perturbatively controlled and makes negligible modification to the bare couplings, provided

$$U\ll\frac{t}{\ln(k_F/\Lambda)}. \tag{2.15}$$

Assuming Eq. (2.15) is satisfied, the remaining fields have longitudinal momentum in only a narrow shell near the Fermi points. Within each shell, we can define chiral (right and left moving) fermions as

$$\psi_{i\alpha}\sim\psi_{Ri\alpha}e^{ik_{Fi}x}+\psi_{Li\alpha}e^{-ik_{Fi}x} \quad \text{for OBC's;} \tag{2.16}$$

$$\psi_{i\alpha}\sim\psi_{Ri\alpha}e^{ik_{Fi}x}+\psi_{L\bar{i}\alpha}e^{-ik_{Fi}x} \quad \text{for PBC's.} \tag{2.17}$$

Here we have introduced the notation $\bar{i}=-i$, which we will continue to use throughout the remainder of the paper. With this definition, ψ_{Ri},ψ_{Li} have opposite momenta in the PBC case (where transverse momentum is a good quantum number). The fields ψ_{Ri},ψ_{Li} may be thought of as ''slowly varying,'' due to their restricted range of momenta.

For small Λ, the dispersion may be linearized within each momentum shell. The effective Hamiltonian is then

$$H_0=\sum_{i,\alpha}\int dx\,v_i[\psi_{Ri\alpha}^{\dagger}i\partial_x\psi_{Ri\alpha}-\psi_{Li\alpha}^{\dagger}i\partial_x\psi_{Li\alpha}], \tag{2.18}$$

where $v_i=2t\,\sin k_{Fi}$.

As it stands, the problem is formulated as an N_f-channel interacting 1D Fermion system. It will sometimes be useful, however, to view the system instead as a finite-width strip of a two-dimensional Hubbard model. To translate between the two pictures, we recognize that in a finite-size system, only a discrete set of transverse momenta k_{yi} are allowed. One may think of these momenta as ''cutting'' the 2D Fermi surface, the intersections being the 1D Fermi points as shown in Figs. 1, 2. This gives an intuitive connection to more familiar two-dimensional physics, and also helps in identifying the possible four-fermion interactions. One caveat that should be kept in mind, however, is that for OBC's, the standing-wave transverse eigenfunctions are linear combinations of momenta $\pm k_{yi}$, so that a single pair of 1D Fermi points corresponds in this case loosely to *four* points on the 2D Fermi surface.

We now try to write down all possible four-point interaction terms allowed by symmetry. In addition to the

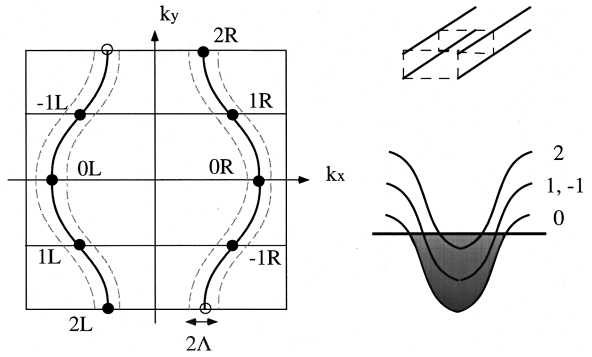

FIG. 1. Band structure of the four-chain Hubbard model with PBC's. Mapping onto the 2D BZ is shown at the left-hand side. The configuration of chains in real space is shown in the upper right.

U(1)×SU(2) symmetry corresponding to charge and spin conservation, these terms must be preserved by charge conjugation, time reversal, parity, and spatial translation operations. The most general particle-conserving four-point vertex has the form

$$H_{\rm int}=\int\prod_a \frac{dk_a}{2\pi}\sum_{P_a,i_a}\delta_{\mathbf{R}}(\boldsymbol{Q})V[\{P_a,i_a,k_a\}] \times\psi^\dagger_{P_1i_1}(k_1)\psi^\dagger_{P_2i_2}(k_2)\psi_{P_3i_3}(k_3)\psi_{P_4i_4}(k_4), \tag{2.19}$$

where $P_i=\pm1\leftrightarrow(R/L)$, and spin indices are left implicit. The fermion fields $\psi_{P_ai_a}(k_a)$ are Fourier transforms of the slowly varying chiral fields defined in Eqs. (2.16) and (2.17). The strengths of the couplings are denoted by $V[\{P_a,i_a,k_a\}]$. The total momentum transfer $\boldsymbol{Q}$ is

$$Q_x=-P_1k_{F1}-P_2k_{F2}+P_3k_{F3}+P_4k_{F4}-k_1-k_2+k_3+k_4, \tag{2.20}$$

$$Q_y=\frac{2\pi}{N}(-P_1i_1-P_2i_2+P_3i_3+P_4i_4)\quad(\text{PBC}). \tag{2.21}$$

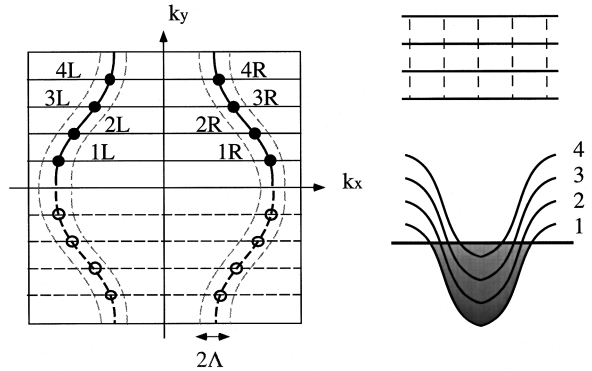

FIG. 2. Band structure of four-chain Hubbard model with OBC's. Since the actual transverse eigenstates with OBC's are standing-wave superpositions containing both $\pm k_y$, we have indicated each 1D Fermi point by two points (one closed and one open circle above) on the BZ. The spatial configuration of chains is shown in the upper right.

Note that Q_y only appears for PBC's, since for OBC's, transverse momentum is not a good quantum number. Momentum conservation is implemented by the lattice δ function

$$\delta_{\mathbf{R}}(\boldsymbol{Q})=\begin{cases}\displaystyle\sum_{n_x}\delta(Q_x-2\pi n_x) & (\text{OBC's})\\ \displaystyle\sum_{n_x,n_y}\delta^{(2)}[\boldsymbol{Q}-2\pi(n_x,n_y)] & (\text{PBC's}),\end{cases} \tag{2.22}$$

where n_x,n_y are integers. Vertices with nonzero **n** are called umklapp interactions.

The dependence of the vertex function on k_a is analyzed via the Taylor expansion (we will assume it is differentiable)

$$V[\{P_a,i_a,k_a\}]=V[\{P_a,i_a,0\}]+\sum_a k_a\frac{\partial V}{\partial k_a}+O(k^2). \tag{2.23}$$

We will see that, while the leading term is *marginal* in the RG sense, all the higher derivative corrections are in fact *irrelevant*, and can be neglected to the (leading) order of accuracy desired here.

A. Interactions for OBC's

Having obtained a general expression [Eq. (2.19)] embodying the constraints on allowed vertices, we now turn to the classification of the solutions of these constraints in the particular cases of interest. We will do this first for the case of OBC's, proceeding in two steps. First, we locate the possible combinations of the band indices $\{P_a,i_a\}$, and second, we determine possible combinations of spin indices, which are implicit in Eq. (2.19), by SU(2) symmetry. Constraints from other symmetries are also discussed.

For OBC's, only momenta in the k_x direction is conserved. We will assume Λ is sufficiently small that the internal momenta k_i may be neglected in Eq. (2.20). The condition for validity of this assumption will be derived at the end of the section.

Since $k_{Fi}\leqslant\pi$, n_x can take values, 0, ±1, ±2. For $n_x=\pm2$, all the Fermi momenta $k_{Fi}=\pi$. This means that these bands must be completely filled, and, following the reasoning described earlier, do not survive in the low-energy theory. For $n_x=\pm1$, momentum balance is possible in partially filled bands. However, at generic fillings, the Fermi momenta are incommensurate (in units of 2π), and cannot be made to sum up to $\pm2\pi$. More careful consideration shows that such interactions only exist on specific umklapp lines in the $(n,t_\perp/t)$ plane. In this paper, we will restrict ourselves to the study of generic fillings, for which these umklapp interactions in the k_x direction may be neglected.

The last kind of vertices with $n_x=0$ conserve x momenta exactly. They may be found by plotting the interactions on the 2D Brillouin zone (BZ). These vertices satisfy

$$Q_x(n,t_\perp)=-P_1k_{F1}-P_2k_{F2}+P_3k_{F3}+P_4k_{F4}=0. \tag{2.24}$$

For a generic Fermi surface, two familiar classes of interactions are *always* allowed. The first comprises forward-scattering interactions, which satisfy

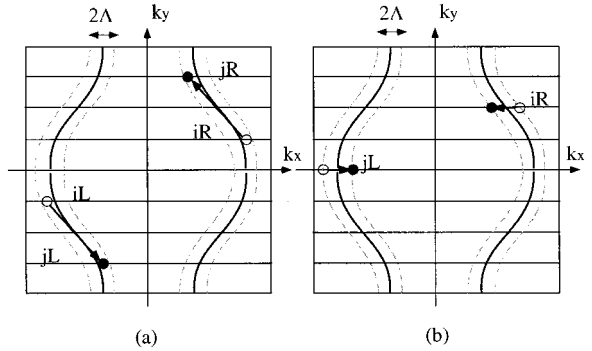

FIG. 3. Examples of Cooper scattering c_{ij} [part (a)] and forward scattering f_{ij} [part (b)].

$$(P_1,P_2)=(P_3,P_4)$$

$$(i_1,i_2)=(i_3,i_4) \quad \text{forward scattering.} \tag{2.25}$$

The second set is the Cooper (or backscattering) channel, defined by

$$P_1=\overline{P_2},P_3=\overline{P_4};$$

$$i_1=i_2,i_3=i_4 \quad \text{Cooper scattering.} \tag{2.26}$$

In Eqs. (2.25) and (2.26), and in the remainder of the paper, $P\equiv -P$ and $(x_1,x_2)=(x_3,x_4)$ indicates pairwise equality, i.e., either $x_1=x_3$, $x_2=x_4$ or $x_1=x_4$, $x_2=x_3$. The two possible solutions for forward scattering actually describe the same vertices, up to a sign from the fermion ordering. Referring to the 2D BZ (see Fig. 3), one sees that forward-scattering interactions conserve the particle number separately in each band, i.e., one electron is annihilated and created in each of the bands i_1 and i_2. In the Cooper-scattering channel, however, a pair of electrons is annihilated in band i_1 and then scattered into band i_3.

There are, however, other vertices at specific fillings. These vertices correspond to special nontrivial solutions of Eq. (2.24). Such solutions exist only on specific lines in the $(n,t_\perp/t)$ plane. Because these lines form a set of measure zero in the full phase space, the corresponding $V[\{P_a,i_a\}]$ will be denoted ''minor'' vertices. Like the umklapp interactions, these minor vertices can be excluded at generic fillings.

We have obtained the allowed vertices in momentum space. However, since the couplings are not momentum dependent, they can equally well be written in terms of a local Hamiltonian density in coordinate space, i.e.,

$$\mathcal{H}_{\rm int}=\sum_{P_a,i_a}\{F[\{P_a,i_a\}]\psi^\dagger_{P_1i_1}\psi^\dagger_{P_2i_2}\psi_{P_1i_1}\psi_{P_2i_2} + C[\{P_a,i_a\}]\psi^\dagger_{P_1i_1}\psi^\dagger_{\overline{P_1i_1}}\psi_{P_2i_2}\psi_{\overline{P_2i_2}}\}, \tag{2.27}$$

where all the ψ and $\psi^\dagger$ are evaluated at the same space point. We have made the classification into forward and Cooper-scattering channels explicit by the change of notation $V[\{P_a,i_a,0\}]\to F[\{P_a,i_a\}],C[\{P_a,i_a\}]$, as appropriate. In the case of forward scattering, as remarked earlier, the two solutions of Eq. (2.24) lead to a single F vertex.

Each vertex obtained so far has several possible generalizations once the spin indices are included. To make them explicit, we now introduce charge and spin currents, in the scalar and vector representations of SU(2), respectively. These are

$$J_{ij}=\psi^\dagger_{i\alpha}\psi_{j\alpha}, \quad \mathbf{J}_{ij}=\frac{1}{2}\psi^\dagger_{i\alpha}\boldsymbol{\sigma}_{\alpha\beta}\psi_{j\beta}, \tag{2.28}$$

where $\boldsymbol{\sigma}$ denote Pauli matrices. These currents satisfy so-called Kac-Moody algebras, and this notation is therefore often referred to as current algebra. To regularize the composite operators in Eq. (2.28), the currents are further defined to be normal ordered (although we do not indicate the normal ordering explicitly). Four-point vertices can be written down as products of two currents. Such bilinear current-current interactions are SU(2) scalars (as appropriate for the Hamiltonian density) if and only if they are formed by coupling two charge or two spin currents. Each vertex in Eq. (2.27) has two counterparts once spin is included. The subset of these which couple right and left movers is

$$-\mathcal{H}^{(1)}_{\rm int}=-\tilde{c}^\rho_{ij}J^R_{ij}J^L_{ij}+\tilde{c}^\sigma_{ij}\mathbf{J}^R_{ij}\cdot\mathbf{J}^L_{ij}, \quad -\tilde{f}^\rho_{ij}J^R_{ii}J^L_{jj}+\tilde{f}^\sigma_{ij}\mathbf{J}^R_{ii}\cdot\mathbf{J}^L_{jj}, \tag{2.29}$$

where $\tilde{f}_{ij}$ and $\tilde{c}_{ij}$ denote the forward and Cooper scattering amplitudes, respectively, between bands i and j. Summation on i,j is implied.

Since f_{ii},c_{ii} describe the same vertex, we choose the diagonal piece of the forward-scattering amplitude to vanish, i.e., $\tilde{f}_{ii}=0$, to avoid double countings. Under charge conjugation $J_{ij}\to J_{ji}$, which implies $\tilde{c}_{ij}=\tilde{c}_{ji}$. Similarly, reflection symmetry (in x) implies $\tilde{f}_{ij}=\tilde{f}_{ji}$. While it is not obvious at this point, the choice of signs for the scalar and vector couplings in Eq. (2.29) such that they are all positive for repulsive on-site interactions.

There are other interactions which are completely chiral, e.g., $J^R_{ii}J^R_{jj}$. As is well known in conformal field theory, such purely chiral interactions do not renormalize or generate renormalization at leading order, and can be neglected in our weak-coupling analysis. Physically, they modify slightly the ''velocities'' of various charge and spin modes, which are already order one in the bare theory.

B. Interactions for PBC's

When PBC's are imposed instead of OBC's, the system retains a finite set of discrete transverse translational symmetry operations. Correspondingly, the transverse momentum k_y (or more properly the exponential e^{ik_y}) is a good quantum number, and the allowed interactions are further constrained by the requirement $Q_y=2\pi n_y$. Since $k_{Fi},k_{yi}\leqslant\pi$, n_x,n_y can take the values, 0, ±1, ±2. As explained in the last subsection, vertices with $n_x=\pm2$ can be ignored in the low-energy theory and those with $n_x=\pm1$ only live on specific umklapp lines and thus are not included. It follows that in the small U limit at generic fillings, it is sufficient to consider only vertices with $\mathbf{n}=(0,0),(0,\pm1),(0,\pm2)$, which conserve the x momenta *exactly*.

The allowed vertices are found in two steps. First, we find all possible vertices which conserve x momentum, and then

we rule out some of them by conservation of y momentum. To do the former, first note that under a y reflection $k_y \to -k_y$, which implies the Fermi momenta satisfy $k_{Fi} = k_{F\bar{\imath}}$, where $\overline{\imath} = -i$. This parity constraint, combined with conservation of x momentum alone allows vertices which satisfy

$$(P_1, P_2) = (P_3, P_4), \quad (i_1, i_2) = (\pm i_3, \pm i_4) \tag{2.30}$$

or

$$P_1 = \overline{P_2}, P_3 = \overline{P_4}, \quad i_1 = \pm i_2, \quad i_3 = \pm i_4. \tag{2.31}$$

Note that Eqs. (2.30) and (2.31) differ from their counterparts for OBC's [Eqs. (2.25) and (2.26)] by the extra choice of $\pm$ sign for PBC's. Physically, this arises because with PBC's, plane waves with momenta $\pm k_y$ form two independent allowed transverse eigenfunctions, while only the single standing-wave (superposition of the two) eigenfunctions satisfies OBC's. As before, additional vertices exist on special lines in the phase diagram, but will be ignored here.

Since the y momentum is also conserved, not all of the vertices in Eqs. (2.30) and (2.31) are allowed. Consider first the corresponding constraint for odd N. We must evaluate Eq. (2.21), which can be rewritten as

$$-P_1 i_1 - P_2 i_2 + P_3 i_3 + P_4 i_4 = n_y N. \tag{2.32}$$

Since all the band indices satisfy $|i| \leqslant (N-1)/2$, solutions with $n_y = \pm 2$ do not exist. Furthermore, after substitution of the partial solutions in Eqs. (2.30)and (2.31), a little algebra shows that the left-hand side in Eq. (2.32) is always even, so that no solutions exists for $n_y = \pm 1$ either. Therefore, for the odd-chain systems, we need only consider the vertices which conserve momenta exactly, i.e., with $\mathbf{n} = (0,0)$.

Equation (2.32) for $n_y = 0$ is satisfied if and only if the $+$ sign is chosen in Eqs. (2.30) and (2.31). With this restriction, the allowed interactions are precisely the same forward- and Cooper-scattering ones that occur in the OBC case, and may therefore be described as before by Eq. (2.29).

The situation is more complicated for N even, because solutions of Eq. (2.32) exist with $n_y = \pm 1$ and $n_y = \pm 2$. The latter do not actually introduce any addition complications. This is because for $n_y = \pm 2$, all the band indices must satisfy $|i_a| = N/2$. The bands $i_a = \pm N/2$ are, however, equivalent, since their y momenta differ by 2π. Therefore, the band indices can instead be chosen equal, and then satisfy $n_y = 0$. These $\mathbf{n} = (0,2)$ vertices are thus included in the $\mathbf{n} = (0,0)$ set which will be discussed later.

The difficulty arises when $\mathbf{n} = (0, \pm 1)$, i.e., $n_y = \pm 1$.

$$-P_1 i_1 - P_2 i_2 + P_3 i_3 + P_4 i_4 = \pm N. \tag{2.33}$$

In this case, choosing the $-$ sign in Eqs. (2.30) and (2.31) leads to solutions of Eq. (2.32). The first set of these is similar to the Cooper channel [see Fig. 4(a)], with indices satisfying

$$P_1 = \overline{P_2}, P_3 = \overline{P_4};$$

$$i_1 = \overline{i_2}, i_3 = \overline{i}, \quad i_1 - i_3 = \pm \frac{N}{2}. \tag{2.34}$$

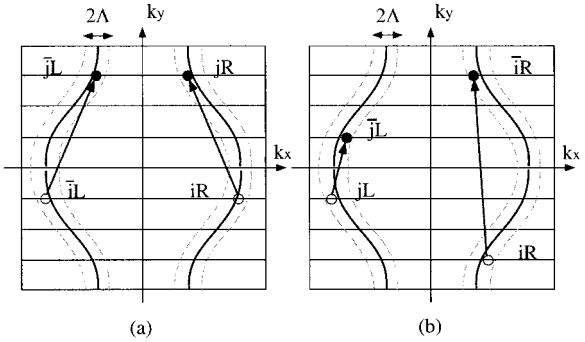

FIG. 4. Examples of transverse umklapp scattering u^1_{ij} [part (a)] and u^2_{ij} [part (b)]. As is clear from the figure, the momentum in the k_y direction is not conserved.

The second set is similar to forward scattering [see Fig. 4(b)], and has

$$(P_1, P_2) = (P_3, P_4);$$

$$(i_1, i_2) = (\overline{i_3}, \overline{i_4}), \quad i_1 - i_2 = \pm \frac{N}{2}. \tag{2.35}$$

The two kinds of umklapp interactions in the k_y direction can also be written down as products of currents. Following the method we developed in last subsection, those y-umklapp interactions which couple the right and left movers can be described by

$$-\mathcal{H}^{(2)}_{\rm int} = -\tilde{u}^{1\rho}_{ij} J^R_{ij} J^L_{\bar{i}\bar{j}} + \tilde{u}^{1\sigma}_{ij} \mathbf{J}^R_{ij} \cdot \mathbf{J}^L_{\bar{i}\bar{j}}, \\ -\tilde{u}^{2\rho}_{ij} J^R_{i\bar{\imath}} J^L_{j\bar{\jmath}} + \tilde{u}^{2\sigma}_{ij} \mathbf{J}^R_{i\bar{\imath}} \cdot \mathbf{J}_{j\bar{\jmath}}. \tag{2.36}$$

Implicit in this notation is the constraint [see Eqs. (2.34) and (2.35)] that the $\tilde{u}_{ij}$ are nonzero only for $|i-j| = (N/2)$. Since $u^1_{i\bar{\imath}}, u^2_{i\bar{\imath}}$ describe the same interaction, we choose $\tilde{u}^{2\rho}_{i\bar{\imath}}, \tilde{u}^{2\sigma}_{i\bar{\jmath}} = 0$ to avoid double counting. Since under charge conjugation, $J_{ij} \to J_{ji}$, $\underline{\tilde{u}_{ij}} = \underline{\tilde{u}}_{ji}$. Similarly, under a parity transformation, $(i,j) \to (\bar{i}, \bar{j})$ and $R \to L$, so $\tilde{u}_{ij} = \tilde{u}_{\bar{i}\bar{j}}$.

Finally, of course, non-umklapp interactions also exist for even N. Just as for N odd, these $\mathbf{n} = (0,0)$ vertices are simply the forward and Cooper channel ones as for OBC's. Therefore, for even-chain systems with PBC's, the full set of allowed vertices comprises forward, Cooper, and $(Q_y = \pm 2\pi)$ umklapp interactions, as given in Eq. (2.29) and Eq. (2.36).

C. Constraints on momentum cutoff

So far, we have determined all the interactions allowed by symmetry, assuming that the momentum cutoff Λ is ''small enough'' to neglect the $-k_1 - k_2 + k_3 + k_4$ term in Eq. (2.20). In this section, we make this requirement precise, and investigate how this begins to break down for larger Λ.

In fact, the results in the last two subsections are strictly correct only for $\Lambda = 0$. With a finite cutoff, the picture is modified in two ways. First, the specific lines on which the ''minor'' couplings exist are widened and occupy a finite area in the $(n, t_\perp/t)$ plane. Second, for sufficiently large Λ, new vertices (not included in the forward and Cooper-scattering channels) can arise for generic fillings [i.e., throughout the $(n, t_\perp/t)$ plane].

Consider first the minor vertices, which exist in the region of the phase diagram defined by

$$f(n,t_\perp;ijkl)\equiv -P_1k_{Fi}-P_2k_{Fj}+P_3k_{Fk}+P_4k_{Fl},$$

$$|f(n,t_\perp;ijkl)|\leqslant 4\Lambda. \tag{2.37}$$

For $\Lambda=0$, as noted previously, solutions of this equation other than the Cooper- and forward-scattering ones exist only on isolated lines. Since $f(n,t_\perp)$ is a smooth function of its arguments, there will be finite neighborhoods around these lines which satisfy Eq. (2.37). The widths δn of these neighborhoods can be estimated by Taylor expanding f around the $f=0$ lines, i.e.,

$$\left|\frac{\partial f}{\partial n}\delta n\right|\sim\Lambda. \tag{2.38}$$

Since the derivatives of the Fermi momenta, $\partial k_F/\partial n$, are of an order of one, the width of the line is approximately as large as the cutoff,

$$\delta n\sim\frac{\Lambda}{k_F}. \tag{2.39}$$

To know the fraction of the phase diagram influenced by these minor vertices, it is also necessary to determine the number (or equivalently, the density) of these regions. Consider first OBC's. Since each region grows adiabatically from a $\Lambda=0$ line, we can simply count the number of solutions to $f(n,t_\perp;ijkl)=0$ (at, say, fixed $t_\perp$). Roughly, the number of solutions may be estimated as follows. Picking a fixed n and $t_\perp$, we choose three of the band indices, say i,j and k. Then $f=0$ determines a Fermi momentum $k_{\rm Fl}$ for the last band. Generally, however, this momentum will not be one of the discrete set of Fermi momenta for this n and $t_\perp$. Now begin varying say $t_\perp$, keeping i,j,k and n fixed. As $t_\perp$ varies, so do k_{Fi},k_{Fj} and k_{Fk}, and hence the required k_{Fl}. As this happens, very soon k_{Fl} will pass through an allowed value, and we have found a solution. Given that, one may then vary *both* $t_\perp$ and n in order to keep $f=0$ for this particular $ijkl$, defining a curve in the $(n,t_\perp/t)$ plane. Since this can be repeated for each set of i,j,k, the total number of such curves is $N_{\rm minor}\sim N^3$. For PBC's, roughly the same argument holds, except that k and l are related by conservation of Q_y. The number of minor vertices for PBC's thus reduces to $N_{\rm minor}\sim N^2$.

For large N, the fraction of the phase diagram in which minor vertices contribute can be estimated simply by summing the widths of these lines. The resulting fraction $f_{\rm minor}\sim N_{\rm minor}\delta n$ is negligible ($f\ll 1$) provided

$$\frac{\Lambda}{k_F}\ll\frac{1}{N^3}\quad\text{(OBC)},$$

$$\frac{\Lambda}{k_F}\ll\frac{1}{N^2}\quad\text{(PBC)}. \tag{2.40}$$

For sufficiently large Λ, the one-dimensional bands associated with adjacent points on the Fermi surface begin to overlap, and it becomes possible to form new interactions by substituting one for the other in the original forward- and

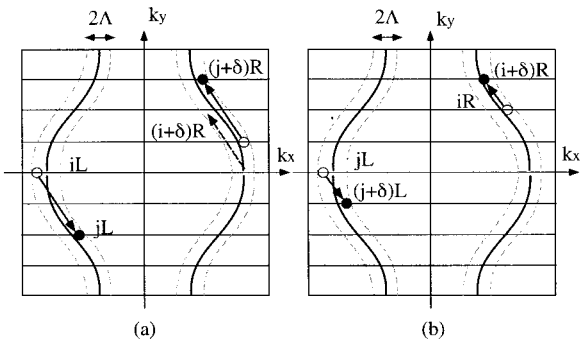

FIG. 5. New vertices for finite cutoff Λ. It is possible to shift the Cooper vertices (shown by dashed lines) for a finite cutoff and still maintain momentum conservation. The maximum shift δ is estimated in Eq. (2.44).

Cooper-scattering channels. If Λ is large enough to allow this, such interactions exist *generically*, i.e., throughout the $(n,t_\perp/t)$ plane. As an example, consider the shifted terms (for PBC's) shown in Fig. 5:

$$-\mathcal{H}^s_{ij}(\delta)=c^\rho_{ij}(\delta)J^R_{i+\delta,j+\delta}J^L_{ij}+f^\rho_{ij}(\delta)J^R_{i,i+\delta}J^L_{j,j+\delta}. \tag{2.41}$$

Here δ parametrizes the transverse momentum shift; for $\delta=0$, the vertices reduce to the familiar Cooper- and forward-scattering types.

Let us consider in detail the conditions under which $\mathcal{H}^s$ conserves momentum in the cutoff theory (see Fig. 5). Because both i and j have been shifted by δ in Eq. (2.41), Q_y is already conserved by design. Taking into account Q_x conservation by Taylor expanding (for $\delta\ll N$), Eq. (2.37) gives the requirement

$$\left|\frac{dk_x}{dk_y}(i)-\frac{dk_x}{dk_y}(j)\right|\frac{2\pi}{N}\delta<\Lambda a. \tag{2.42}$$

To obtain an order of magnitude estimate, we then approximate the mean curvature between bands i,j by its typical value $t_\perp/t$,

$$\left|\frac{dk_x}{dk_y}(i)-\frac{dk_x}{dk_y}(j)\right|\simeq\frac{d^2k_x}{dk_y^2}\frac{2\pi}{N}|i-j|$$

$$\simeq\left(\frac{t_\perp}{t}\right)\frac{2\pi}{N}|i-j|. \tag{2.43}$$

The maximum allowed shift $\delta_{\rm max}$ in band indices is therefore

$$\delta_{\rm max}\sim\left(\frac{t}{t_\perp}\right)\frac{N^2}{|i-j|}\frac{\Lambda}{k_F}. \tag{2.44}$$

For $\delta_{\rm max}<1$, only the unshifted Cooper channel interaction is allowed. Demanding this leads to the constraint

$$\frac{\Lambda}{k_F}<\left(\frac{t_\perp}{t}\right)\left(\frac{1}{N^2}\right). \tag{2.45}$$

Combining the constraint on the initial coupling strengths, Eq. (2.15), and that on the momentum cutoff, Eqs. (2.40), (2.45), we find the reduced set of interactions in Eq. (2.29) and (2.36) is sufficient provided the initial coupling strengths satisfy

$$\frac{U}{t} \ll \frac{1}{\ln N}. \tag{2.46}$$

Here we have dropped the order one factors in front of the logarithm which are different for OBC's and PBC's. Since the condition on U is only logarithmic in N, it is not a severe constraint on the initial values of the couplings for finite chains. Nevertheless, it is clear that the true two-dimensional limit is rather subtle. Indeed, Eq. (2.46) indicates a possible non-commutativity of the order of limits (at zero temperature) in taking $U \to 0$ and $N \to \infty$. We will return to the interesting and important issues involved in the 2D limit in Sec. VI. For the moment, we will restrict ourselves to finite N and discuss the corresponding weak-coupling behavior of such systems, under the conditions of Eq. (2.46).

III. RENORMALIZATION GROUP FLOW EQUATIONS

To analyze the behavior of the weakly interacting system, we employ the RG approach. In this section, we describe the scheme used and present the resulting differential RG flow equations (analogous flow equations for particular restricted cases were obtained in Refs. 35 and 36). Further details of the calculations can be found in Appendix A. The general approach of the RG is to progressively eliminate short-wavelength, high-energy degrees of freedom. To formulate this mode elimination, we first rewrite the partition function in terms of an average,

$$\begin{aligned} Z &= \int [d\overline{\psi}][d\psi] e^{-S_0 - S_{\rm int}} \\ &= Z_0 \langle e^{-S_{\rm int}} \rangle_0, \end{aligned} \tag{3.1}$$

where Z_0 is the partition function without interactions, and angular brackets with the subscript 0 denotes an average with respect to the quadratic action S_0 only. This form may be reexponentiated using the cumulant expansion,

$$\langle e^{-S_{\rm int}} \rangle_0 = \exp\{\langle -S_{\rm int} \rangle_0 + \tfrac{1}{2}[\langle S_{\rm int}^2 \rangle_0 - \langle S_{\rm int} \rangle_0^2] + O(S_{\rm int}^3)\}. \tag{3.2}$$

Up to this point, we have systematically derived the low-energy fermion model with a ''momentum-shell'' cutoff Λ. While the RG may be implemented directly with this model, it happens that the one-loop RG equations needed here are in fact independent of the cutoff scheme used. This independence arises from the dominance of logarithmically divergent terms at one-loop level, whose coefficients are insensitive to the particular form of cutoff used. We take advantage of this property here by adopting instead a real-space cutoff $a \approx 1/\Lambda$. This distance then appears as an explicit cut-off in all x integrals, e.g.,

$$\langle S_{\rm int}^2 \rangle_0 = \int_a^\infty \prod_{i=1,2} d\tau_i dx_i \langle \mathcal{H}_{\rm int}(\tau_1, x_1) \mathcal{H}_{\rm int}(\tau_2, x_2) \rangle_0, \tag{3.3}$$

using the compact notation $\int_A^B \equiv \int_{A<|x_1 - x_2|<B}$. Each integral is now separated into two parts: long-wavelength modes, $|x_1 - x_2| > ba$, and short-wavelength modes, $a < |x_1 - x_2| < ba$, where $b > 1$ is the rescaling parameter. This separation is convenient because in the latter integral, all fields are at nearby space points. This allows the use of the operator product expansion to replace the products of such nearby operators by a series of local operators (for review, see Refs. 37, 38), i.e.,

$$\begin{aligned} &\int_a^{ba} \prod_{i=1,2} d\tau_i dx_i \langle \mathcal{H}_{\rm int}(\tau_1, x_1) \mathcal{H}_{\rm int}(\tau_2, x_2) \rangle_0 \\ &\quad \simeq \int dx\, d\tau \langle \delta\mathcal{H}_{\rm int} \rangle_0. \end{aligned} \tag{3.4}$$

The method to compute the effective interaction, $\delta\mathcal{H}_{\rm int}$, can be found in Appendix A.

As shown in Appendix A, the effective interaction $\delta\mathcal{H}_{\rm int}$ has the same form as the original Hamiltonian, and thus has the effect of renormalizing the bare couplings. The RG finishing with a rescaling step, which attempts to bring the theory as much as possible back to its original form. To restore the original value of the cutoff and maintain the original set of Fermi velocities requires the change of variables

$$x' = \frac{x}{b}, \quad \tau' = \frac{\tau}{b}, \tag{3.5}$$

$$\overline{\psi'}(x, \tau) = b^{1/2} \overline{\psi}(x', \tau'), \quad \psi'(x, \tau) = b^{1/2} \psi(x', \tau'). \tag{3.6}$$

While this indeed preserves (at one-loop order) the form of S_0, the interactions are of course changed. The simplest way to keep track of these changes is to perform the RG *infinitesimally*, with the rescaling factor $b = e^{dl}$. Iterating both steps of the RG then leads to differential RG flow equations for the coupling constants, as a function of length scale $L(l) = e^l$.

For OBC's, the allowed couplings are forward and Cooper scattering. The RG equations governing them are

$$\dot{f}_{ij}^\rho = (c_{ij}^\rho)^2 + \frac{3}{16}(c_{ij}^\sigma)^2, \tag{3.7}$$

$$\dot{f}_{ij}^\sigma = -(f_{ij}^\sigma)^2 + 2c_{ij}^\rho c_{ij}^\sigma - \frac{1}{2}(c_{ij}^\sigma)^2, \tag{3.8}$$

$$\begin{aligned} \dot{c}_{ij}^\rho = &-\sum_k \{\alpha_{ij,k}(c_{ik}^\rho c_{kj}^\rho + \tfrac{3}{16} c_{ik}^\sigma c_{kj}^\sigma)\} \\ &+ (c_{ij}^\rho h_{ij}^\rho + \tfrac{3}{16} c_{ij}^\sigma h_{ij}^\sigma), \end{aligned} \tag{3.9}$$

$$\begin{aligned} \dot{c}_{ij}^\sigma = &-\sum_k \{\alpha_{ij,k}(c_{ik}^\rho c_{kj}^\sigma + c_{ik}^\sigma c_{kj}^\rho + \tfrac{1}{2} c_{ik}^\sigma c_{kj}^\sigma)\} \\ &+ (c_{ij}^\rho h_{ij}^\sigma + c_{ij}^\sigma h_{ij}^\rho - \tfrac{1}{2} c_{ij}^\sigma h_{ij}^\sigma), \end{aligned} \tag{3.10}$$

where $f_{ij} = \widetilde{f}_{ij}/\pi(v_i + v_j)$ and the same for c_{ij}. Also, we define $h_{ij} \equiv 2 f_{ij} + \delta_{ij} c_{ii}$ for convenience. The weight factor in the summation $\alpha_{ij,k} \equiv \{(v_i + v_k)(v_j + v_k)/[2v_k(v_i + v_j)]\}$ is symmetrical in i, j. The dots indicate logarithmic derivatives with respect to the length scale, i.e., $\dot{f} \equiv \partial f / \partial l$.

For PBC's, if the number of chains is odd, the allowed vertices are the same as in OBC, and Eqs. (3.7)–(3.10) hold without modification. However, if the number of chains is even, the additional umklapp interactions in the k_y direction

give rise to additional flow equations and extra terms in the forward and Cooper-scattering equations above. Because these augmented RG equations are quite complicated and do not provide any obvious insights upon inspection, we have relegated them to Appendix B.

Equations (3.7)–(3.10) must be supplemented by initial conditions to completely specify the problem. While it is of course straightforward to obtain these initial values from the bare couplings, it does require a certain amount of algebra to work out the effect of the unitary transformation in Eqs. (2.4) and (2.5) (see Appendix C). Initially, then, all the couplings f_{ij}, c_{ij} are $O(U/t)$ (but with specific ratios).

IV. STRONG-COUPLING ANALYSIS

In this section, we describe the application of the RG equations to the N-chain Hubbard models with both OBC's and PBC's for small N. We will see that the RG flows almost always diverge, and will discuss the interpretation of such divergences, using as input certain general features of the numerical integrations. The instabilities encountered generally correspond to some degree of pairing, the notion of which we make precise through the study of various pair fields.

A. Classification of couplings

1. General scheme

With the initial values in hand, the RG flow equations can be integrated to investigate the physics of the weak-coupling limit. We have done this using Mathematica on a Sun Sparc-4 workstation. While the specific solution found depends upon the details of the model parameters (e.g., N, $t_\perp/t$, n), certain gross features of the behavior are generic. In particular, for almost all sets of initial conditions, the solutions of the RG equations are singular, and certain linear combinations of coupling constants diverge at some *finite* l_d. Since the RG equations were obtained perturbatively, they are not valid arbitrarily close to such an apparent divergence. To obtain sensible results, we instead cutoff the RG flow at some specific length scale $l^* < l_d$, chosen so that $U/t \ll \max\{f_{ij}, c_{ij}, u_{ij}\} \ll 1$. At this cutoff length scale, the couplings may be classified into two groups. The first set includes those couplings which have become ''large'' but still weak, i.e., $U/t \ll g_i \ll 1$, which we call marginally *relevant*. The remaining couplings do not grow under the RG, but remain $O(U/t)$ or smaller, and will be called *marginal* or *marginally irrelevant*, respectively. At the length scale l^*, the system thus exhibits a separation of energy scales, with the marginally relevant interactions much larger than the marginal or marginally irrelevant ones. The phase diagram of the system may then be determined simply by neglecting the latter interactions and studying the states determined by the marginally relevant couplings alone.

2. Strict $U \to 0^+$ limit

In the truly asymptotic limit $U \to 0^+$, much of the classification of couplings can be accomplished analytically. To do so, consider the formal solutions of the RG flow equations as functions of l and the Hubbard interaction U, which we will denote $g_i(l;U)$, where i is a composite index labeling all the interactions. The perturbative RG is valid provided all the *renormalized* interactions are small, i.e., $|g_i(l;U)| \ll 1$, which is certainly true initially. To proceed, we need to assume something about the form of $g_i(l;U)$ near the divergent scale l_d. Assuming a power-law first suggested in Ref. 30 (which can be verified analytically for simple cases and numerically quite generally), dimensional analysis essentially requires

$$g_i(l;U) \simeq \frac{UG_i}{(l_0 - Ul)^{\gamma_i}}, \tag{4.1}$$

where $l_0 = Ul_d$ and we have set $t=1$ here and in the remainder of this section. The order one coefficients G_i and exponents γ_i remain to be determined. Given the form of Eq. (4.1), it is clear that the formally divergent couplings only become much greater than U when l is very close to l_d. We are thus actually interested in the *asymptotic* behavior of Eqs. (3.7)–(3.10). Unlike the full integration of the RG flows, the less ambitious task of determining these asymptotics can in fact be accomplished analytically, as we now demonstrate.

In order to fix the exponents γ_i, it is necessary to use some input from numerics. In particular, in every case we have examined, the vector part of the forward-scattering interactions, f_{ij}^σ, is always marginally *irrelevant*. From Eq. (3.8), this implies that the combination $2c_{ij}^\rho c_{ij}^\sigma - \frac{1}{2}(c_{ij}^\sigma)^2$ is small, i.e., $\lesssim O(U^2)$. Since we are keeping only those interactions which scale to values of order one, to this order of accuracy the renormalized couplings satisfy

$$f_{ij}^\sigma(l^*) \approx 0, \tag{4.2}$$

$$c_{ij}^\sigma(l^*) \approx 4c_{ij}^\rho(l^*) \quad (i \neq j). \tag{4.3}$$

Equations (4.2) and (4.3) suffer corrections of $O(U)$, but may be treated as equalities in the following leading-order analysis.

Equations (4.2) and (4.3) can be understood in a simple physical way. Some simple algebra demonstrates that if Eqs. (4.2) and (4.3) were replaced by exact equalities, these conditions would be preserved by the RG flow. Thus it is natural to suspect that under these conditions, the system has acquired an additional symmetry. Indeed, upon closer examination one finds that the constraint implies *independent* conservation of spin within each band. Although this is not an exact property of the Hubbard model, it is approximately satisfied due to the on-site nature of the interactions. For on-site interactions, Fermi statistics allow only a coupling of oppositely oriented spins, which implies Eq. (4.3). Apparently the deviation from this symmetry caused by the nonzero initial values of f_{ij}^σ is sufficiently small to allow the symmetry to be asymptotically restored at long distances.

Based on this observation, we will calculate the exponents γ_i in the $U \to 0^+$ limit, taking as an example the Cooper-scattering vertices. Other exponents can be obtained by similar means. The RG equations for the Cooper couplings c_{ii}^σ in Eq. (3.9) can be rewritten with the help of Eq. (4.3) as

$$\dot{c}_{ii}^\sigma \approx -(c_{ii}^\sigma)^2 - \sum_{k \neq i} \alpha_{ii,k}(c_{ik}^\sigma)^2. \tag{4.4}$$

Since all terms on the right-hand side are of the same sign (negative), they cannot cancel one another, and balancing the two sides of the equation then gives the constraint

$$\gamma_{ii}^{c\sigma}+1=\max\{2\gamma_{ii}^{c\sigma},2\gamma_{ik}^{c\sigma}\}, \tag{4.5}$$

where $\gamma_{ij}^{c\sigma}\equiv\gamma(c_{ij}^{\sigma})$.

Equation (4.5) has two solutions. The first is

$$\gamma_{ik}^{c\sigma}\leqslant\gamma_{ii}^{c\sigma}=1. \tag{4.6}$$

The second possibility is

$$\gamma_{ii}^{c\sigma}<\gamma_{ik}^{c\sigma}=(1+\gamma_{ii}^{c\sigma})/2\leqslant 1. \tag{4.7}$$

We thus conclude that all the exponents associated with Cooper couplings are bounded above by one. Similar considerations applied to the other RG equations imply that *all* the exponents are less than or equal to one. If one can probe arbitrarily near the divergent point l_d (i.e., if U is put arbitrarily close to 0^+), any couplings with exponents $\gamma_i=1$ will eventually outstrip any others with smaller exponents (even those with larger prefactors). In the strict $U\to 0^+$ limit, therefore, the relevant couplings are those with exponents $\gamma_i=1$.

From Eq. (4.1), the relevant couplings with initial interaction U thus satisfy

$$g_i(l;U)\simeq\frac{UG_i}{l_0-Ul}, \tag{4.8}$$

for l near the cutoff length scale l_d. Substituting Eq. (4.8) into Eqs. (3.7)–(3.10), the parameters U and l_d cancel out, leaving a set of *algebraic* relations between the *constants* G_i. These algebraic equations are formally obtained from Eqs. (3.7)–(3.10) simply by replacing $g_i\to G_i$ and $\dot{g}_i\to G_i$. The relative strengths of various couplings in the asymptotic regime can then be determined (relatively) easily using these algebraic relations. Usually there is more than one solution for G_i. The identification of specific solutions with specific initial conditions which depend on, e.g., filling factor n, can only be found using numerical integration of the full RG equations. We emphasize as well that these results rely upon the strict $U\to 0^+$ limit. *A priori*, given the lack of other energy scales in the Hubbard model, we would nevertheless expect such results to hold qualitatively provided $U\lesssim 1$ (for fixed small finite N). In fact, given the large number of coupling constants involved, apparently order one factors can conspire to render the limits of validity of this strict weak-coupling limit considerably smaller (e.g., $U/t\lesssim 10^{-5}$ in some regions of the phase diagram even for $N=2$—see Sec. V). For $U/t\lesssim 1$ but *outside* the strict $U\to 0^+$ limit, the algebraic relations do not hold, but we nevertheless expect quantitatively correct results from the *numerical* integration of the full RG flows.

B. Bosonization strategy

Our strategy will be to bosonize relevant couplings in the renormalized Hamiltonian at the scale l^*. This is done using the bosonization formula[39,40]

$$\psi_{R/Li\alpha}(l^*)=\sqrt{\frac{\Lambda}{2\pi}}\,\eta_{i\alpha}e^{(i\sqrt{4\pi}\phi_{R/Li\alpha})}. \tag{4.9}$$

Here the chiral boson fields $\phi_{R/Li\alpha}$ obey the commutation relations

$$[\phi_{Ri\alpha}(x),\phi_{Rj\beta}(y)]=-[\phi_{Li\alpha}(x),\phi_{Lj\beta}(y)]=\frac{i}{4}\,\mathrm{sgn}(x-y)\,\delta_{ij}\delta_{\alpha\beta}, \tag{4.10}$$

$$[\phi_{Ri\alpha}(x),\phi_{Lj\beta}(y)]=\frac{i}{4}. \tag{4.11}$$

The $\eta_{i\alpha}$ are Majorana (real) fermions, known as Klein factors, introduced to preserve the proper anticommutation relations between fermion fields with differing band and spin indices. They obey

$$\{\eta_{i\alpha},\eta_{j\beta}\}=2\,\delta_{ij}\delta_{\alpha\beta}. \tag{4.12}$$

It is usually more convenient to trade the chiral boson fields pairwise for a conventional bosonic phase field ϕ and its dual (displacementlike) field θ, defined by

$$\phi_{i\alpha}=\phi_{Ri\alpha}+\phi_{Li\alpha},$$

$$\theta_{i\alpha}=\phi_{Ri\alpha}-\phi_{Li\alpha}. \tag{4.13}$$

They satisfy $[\phi(x),\theta(y)]=-i\Theta(y-x)$. Physically, the $\theta(x)$ field describes the displacement of the electrons, while the dual field $\phi(x)$ represents their phase. We can make a further canonical transformation to

$$(\phi,\theta)_{i\rho}=[(\phi,\theta)_{i\uparrow}+(\phi,\theta)_{i\downarrow}]/\sqrt{2},$$

$$(\phi,\theta)_{i\sigma}=[(\phi,\theta)_{i\uparrow}-(\phi,\theta)_{i\downarrow})]/\sqrt{2}. \tag{4.14}$$

The ρ fields then describe charged singlet excitations, while the σ fields describe neutral excitations carrying spin. Carrying through the change of variables in Eq. (4.9) carefully, one finds that the noninteracting Hamiltonian Eq. (2.18) is equivalent to the bosonic Euclidean action

$$S_0=\sum_{i\nu}\int_{x,\tau}\frac{v_i}{2}[(\partial_x\phi_{i\nu})^2+(\partial_x\theta_{i\nu})^2]+i\,\partial_x\theta_{i\nu}\partial_\tau\phi_{i\nu}, \tag{4.15}$$

where $\nu=\rho,\sigma$.

Upon bosonizing with Eq. (4.9), the four-fermion interactions are converted to linear combinations of gradient couplings and sinusoidal functions of the phases. The former give rise to continuous shifts of the parameters of the low-energy description: modifications of mode velocities, charge stiffnesses, etc. We say that these shifts leave the system in the same *phase*. The sinusoidal interactions, by contrast, can potentially cause more drastic changes in the low-energy theory. They tend to ''pin'' their arguments (linear combinations of the bosonic phases) to particular values, modulo 2π. We will treat the marginally relevant couplings in this way, by *expanding* the corresponding harmonic functions around their minima, regarding the fluctuations around them as mas-

sive. This will effectively give gaps to some of the modes of the original noninteracting fermion system, resulting in distinct new phases.

To perform this procedure and determine the nature of the gaps arising from the interactions, then, it is sufficient to keep only those marginally relevant couplings which become sinusoids upon bosonization. There are still quite a number of potential such terms, so it now pays to use some additional input from the numerics.

C. Generic instability

For simplicity, we will first focus on situations in which the relevant couplings include only forward- (f) and cooper- (c) scattering vertices. This is completely general for OBC's, but excludes certain regions of phase space in the case of PBC's with even N, for which the transverse umklapp (u) couplings may become relevant. This alternate channel of instability will be returned to later in this section.

1. Semiclassical Hamiltonian and analysis

As a preliminary step in the analysis, we first rewrite the interactions in terms of the underlying fermion fields. Using the SU(2) identity,

$$\boldsymbol{\sigma}_{\alpha\beta}\cdot\boldsymbol{\sigma}_{\gamma\epsilon}=2\,\delta_{\alpha\epsilon}\delta_{\beta\gamma}-\delta_{\alpha\beta}\delta_{\gamma\epsilon}, \tag{4.16}$$

the scalar and vector parts from Eq. (2.29) become

$$\begin{aligned}\mathcal{H}^{(1)}_{\rm int}=\sum_{ij}\ [&f^{\rho}_{ij}\psi^{\dagger}_{Ri\alpha}\psi_{Ri\alpha}\psi^{\dagger}_{Lj\beta}\psi_{Lj\beta}\\&+(c^{\rho}_{ij}+\tfrac{1}{4}c^{\sigma}_{ij})\psi^{\dagger}_{Ri\alpha}\psi_{Rj\alpha}\psi^{\dagger}_{Li\beta}\psi_{Lj\beta}\\&-\tfrac{1}{2}c^{\sigma}_{ij}\psi^{\dagger}_{Ri\alpha}\psi_{Rj\beta}\psi^{\dagger}_{Li\beta}\psi_{Lj\alpha}].\end{aligned} \tag{4.17}$$

Here we have dropped the irrelevant forward scattering f^{σ}_{ij}.

Following the strategy above, we must now bosonize the system. In doing so, the interactions in Eq. (4.17) may be divided into two sets. The first consists of f^{ρ}_{ij} and c^{ρ}_{ii}, which only contribute gradient terms after bosonization. To determine the phase of the system, therefore, we need include only the second set, which contains the Cooper couplings c^{σ}_{ii}, c^{σ}_{ij}, and c^{ρ}_{ij}. Keeping only these terms, and imposing the constraint in Eq. (4.3), the interaction Hamiltonian becomes

$$\begin{aligned}\mathcal{H}^{(1)}_{\rm int}=&\sum_{i}\ \frac{1}{2}c^{\sigma}_{ii}\psi^{\dagger}_{Ri\alpha}\psi^{\dagger}_{Li\bar{\alpha}}\psi_{Ri\bar{\alpha}}\psi_{Li\alpha}\\&+\sum_{i\neq j}\ \frac{1}{2}c^{\sigma}_{ij}[\psi^{\dagger}_{Ri\alpha}\psi^{\dagger}_{Li\bar{\alpha}}\psi_{Rj\bar{\alpha}}\psi_{Lj\alpha}\\&+\psi^{\dagger}_{Ri\alpha}\psi^{\dagger}_{Li\bar{\alpha}}\psi_{Lj\bar{\alpha}}\psi_{Rj\alpha}],\end{aligned} \tag{4.18}$$

where $\bar{\alpha}\equiv-\alpha$. The interactions with $\alpha=\beta$ in the third and fourth terms in Eq. (4.17) aforementioned independent conservation of spin in channels i and j. This ordering of fermion fields is particularly convenient for bosonization.

As shown in detail in Appendix D, for this set of interactions the Klein factors can be represented by the identity $\eta_i=1$. Inserting Eq. (4.9) in Eq. (4.18), we then obtain

$$\begin{aligned}\mathcal{H}^{(1)}_{\rm int}\sim&\sum_{i}\ c^{\sigma}_{ii}\cos(\sqrt{8\pi}\theta_{i\sigma})\\&+\sum_{i<j}\ 4c^{\sigma}_{ij}\cos(\sqrt{4\pi}\phi^{\rho-}_{ij})\cos(\sqrt{2\pi}\theta_{i\sigma})\cos(\sqrt{2\pi}\theta_{j\sigma}),\end{aligned} \tag{4.19}$$

where $\phi^{\rho\pm}_{ij}\equiv(\phi^{\rho}_{i}\pm\phi^{\rho}_{j})/\sqrt{2}$. As pointed out by Schulz,[26] this explicit form after bosonization depends on the representation chosen for the Klein factors. In other words, we still have some ''gauge'' freedom left to shift the bosonic fields. However, the physical correlation functions, which include these Klein factors, are independent of the specific gauge choice.

We next locate the minima of Eq. (4.19). These can *a priori* be nontrivial, but turn out to be very simple in practice. In fact, we find that in all cases, the numerically determined values of the coefficients c^{σ}_{ii} and c^{σ}_{ij} are such that each term in Eq. (4.19) can be minimized *separately*. Most often this occurs because all the relevant couplings occur in channels connecting only two specific bands. We will focus on this special case now, in order to present a more detailed but containable exposition.

To proceed, let us denote the indices of the two strongly interacting bands by a and b. The numerical integration demonstrates that, although they are initially positive (repulsive interactions), the diagonal Cooper-scattering spin vertices are driven negative under the RG. That is

$$c^{\sigma}_{aa},c^{\sigma}_{bb}<0. \tag{4.20}$$

We also obtain the sign

$$c^{\sigma}_{ab}=4c^{\rho}_{ab}>0. \tag{4.21}$$

Given these signs, a global minimum of Eq. (4.19) is

$$\sqrt{2\pi}\langle\theta_{a\sigma}\rangle=l\pi, \tag{4.22}$$

$$\sqrt{2\pi}\langle\theta_{b\sigma}\rangle=m\pi, \tag{4.23}$$

$$\sqrt{4\pi}\langle\phi^{\rho-}_{ab}\rangle=(l+m+2n+1)\pi, \tag{4.24}$$

where l,m,n are integers. Since all solutions give the same results of correlation functions, we will pick the $l=m=n=0$ solution for convenience. Fluctuations around this semiclassical solution are massive, as can be seen by the change of variables

$$\theta_{a\sigma}=\langle\theta_{a\sigma}\rangle+\delta\theta_{a\sigma}, \tag{4.25}$$

$$\theta_{b\sigma}=\langle\theta_{b\sigma}\rangle+\delta\theta_{b\sigma}, \tag{4.26}$$

$$\phi^{\rho-}_{ab}=\langle\phi^{\rho-}_{ab}\rangle+\delta\phi^{\rho-}_{ab}. \tag{4.27}$$

Expanding to quadratic order gives

$$\begin{aligned}\mathcal{H}^{(1)}_{\rm int}\sim&\frac{1}{2}(m^{\sigma}_{a})^2(\delta\theta_{a\sigma})^2+\frac{1}{2}(m^{\sigma}_{b})^2(\delta\theta_{b\sigma})^2\\&+\frac{1}{2}(m^{\rho}_{ab})^2(\delta\phi^{\rho-}_{ab})^2,\end{aligned} \tag{4.28}$$

up to a constant. The masses for spin and charge modes are

$$m_a^\sigma = 2\sqrt{2\pi}(|c_{aa}^\sigma| + c_{ab}^\sigma)^{1/2}, \tag{4.29}$$

$$m_b^\sigma = 2\sqrt{2\pi}(|c_{bb}^\sigma| + c_{ab}^\sigma)^{1/2}, \tag{4.30}$$

$$m_{ab}^\rho = 4\sqrt{\pi}(c_{ab}^\sigma)^{1/2}. \tag{4.31}$$

Comparison with the corresponding quadratic frequency terms in the noninteracting action [Eq. (4.15)] indicates that Eq. (4.28) describes three *gapful* modes, $\theta_{a\sigma}$, $\theta_{b\sigma}$, and $\phi_{ab}^{\rho-}$. The first two terms in Eq. (4.28) suppress fluctuations in the spin densities of the two channels, and correspond to spin gaps with magnitudes proportional to m_a^σ and m_b^σ. The third term ''locks'' together the relative phase of the charge modes in the two channels. The remaining linear combination $\phi_{ab}^{\rho+}$ and its conjugate $\theta_{ab}^{\rho+}$ are not affected by $\mathcal{H}_{\rm int}^{(1)}$, and continue to describe a gapless total charge mode.

2. Pair fields

The existence of a spin gap naturally suggests pairing of electrons with oppositely oriented spins. To investigate this notion further, it is instructive to consider a pairing operator

$$\hat{\Psi}(X,x) = \psi_{Pi\alpha}(X+x/2)\psi_{P'j\beta}(X-x/2), \tag{4.32}$$

which annihilates two electrons with specified band indices and spin at particular positions. For compactness, we will omit explicit labeling of the pairing operator $\hat{\Psi}$ unless necessary to avoid ambiguity. In a true superconductor, such pair fields *condense*, so that $\langle\hat{\Psi}\rangle \neq 0$. The Mermin-Wagner theorem prohibits such a continuous symmetry breaking in $1+1$ dimensions, but $\hat{\Psi}$ can have power-law correlations (quasi-long-range order). Of physical interest are correlation functions of two or more of the various $\hat{\Psi}$ operators at different well-separated points (in X). For instance,

$$C_{AB}(X,x) = \langle \hat{\Psi}_A^\dagger(X,x)\hat{\Psi}_B(0,x)\rangle, \tag{4.33}$$

where the composite index $A=(P_A i_A \alpha_A, P_A' j_A \beta_A)$, and B is defined in the same way. Following the RG strategy, correlation functions such as $C_{AB}(x)$ are evaluated in several steps. First, we employ the perturbative RG, integrating out fermion modes until the scale l^*. Ignoring perturbative corrections from the mode integration, each pairing operator then picks up just the rescaling factor

$$\hat{\Psi}(X,x) \approx \frac{1}{\Lambda\xi}\,\hat{\Psi}(X/\Lambda\xi, x/\Lambda\xi; l^*), \tag{4.34}$$

where we have defined the *coherence length* $\xi = \Lambda^{-1}e^{l^*}$. At this point, the relevant couplings have become of order one, and may be safely bosonized. Carrying this out gives

$$\hat{\Psi}(X,x) \simeq \frac{1}{\Lambda\xi}\,\eta_{i\alpha}\eta_{j\beta}\exp[i\sqrt{4\pi}\{\phi_{Pi\alpha}[(X+x/2)/\Lambda\xi] + \phi_{P'j\beta}[(X-x/2)/\Lambda\xi]\}]. \tag{4.35}$$

The next step is to insert this in the desired correlation function, e.g., Eq. (4.33), and integrate out the massive modes using Eq. (4.28). Since the masses in Eq. (4.28) are order one, the correlation functions of the gapped phase variables will decay exponentially over (rescaled) distances of order one. This allows us to make the requirement of ''well-separated'' points more precise. Since the internal coordinates of the fields have themselves been rescaled by ξ, it follows that for $|X| \gg \xi$, the massive phase variables in two pair fields separated by a distance $|X|$ are exponentially decorrelated (provided the ''internal'' coordinates satisfy $|x| \ll |X|$), and may be integrated out independently for each $\hat{\Psi}$. For instance,

$$\langle \hat{\Psi}_A^\dagger(X,x)\hat{\Psi}_B(0,x')\rangle_g \approx \langle \hat{\Psi}_A^\dagger(X,x)\rangle_g \langle \hat{\Psi}_B(0,x')\rangle_g, \tag{4.36}$$

for $|X| \gg \xi$, where the subscript g indicates an average over the gapped phase fields.

It is thus sufficient to study the partially averaged pairing operators $\langle\hat{\Psi}(X,x)\rangle_g$. We will do this carefully for the case of the two bands a and b. The average is carried out with respect to the action $S = \tilde{S}_0 + S_1$, where

$$\tilde{S}_0 = \sum_s \int_{x,\tau} \frac{v_i}{2}[(\partial_x\phi_s)^2 + (\partial_x\theta_s)^2] + i\partial_x\theta_s\partial_\tau\phi_s, \tag{4.37}$$

where $s = a\sigma, b\sigma, ab\rho-$, as obtained from Eq. (4.15), and

$$S_1 = \int_{x,\tau} \mathcal{H}_{\rm int}^{(1)}. \tag{4.38}$$

From Eqs. (4.28) and (4.37), the small deviations $\delta\theta_{a\sigma}$, $\delta\theta_{b\sigma}$, and $\delta\phi_{ab}^{\rho-}$ are decoupled (from each other, but not from their conjugate fields) at the quadratic level, and may therefore be averaged independently.

In carrying out this average, it is important to note the appearance of the conjugate fields $\delta\phi_{a\sigma}$, $\delta\phi_{b\sigma}$, and $\delta\theta_{ab}^{\rho-}$. By the uncertainty principle, since $[\phi,\theta] = O(1)$, these variables are wildly fluctuating. This implies that any complex exponential containing one of these fields will average to zero, unless it appears in the form of a ''neutral'' difference at nearby points, in which its fluctuation mean value is automatically subtracted. If such a subtraction does occur, the average will decay exponentially with the separation of the subtracted fields.

In fact, only four pairing operators satisfy this strong neutrality constraint, and are therefore nonvanishing. These are

$$\langle \hat{\Psi}_{d+}(X,x)\rangle_g = (\Lambda\xi)^{-1}\langle \psi_{Rd\uparrow}[(X+x/2)/\Lambda\xi] \times \psi_{Ld\downarrow}[(X-x/2)/\Lambda\xi]\rangle_g,$$

$$\langle \hat{\Psi}_{d-}(X,x)\rangle_g = (\Lambda\xi)^{-1}\langle \psi_{Rd\downarrow}[(X+x/2)/\Lambda\xi] \times \psi_{Ld\uparrow}[(X-x/2)/\Lambda\xi]\rangle_g, \tag{4.39}$$

where again $d = a,b$. As expected, only electrons with opposite spin tend to form pairs.

Inserting Eq. (4.35) into Eq. (4.39), we obtain three averages. In the relative charge sector,

$$\left\langle \exp\left(\pm i\frac{\sqrt{\pi}}{2}[\phi_{ab}^{\rho-}(\chi/2) + \phi_{ab}^{\rho-}(-\chi/2) + \theta_{ab}^{\rho-}(\chi/2)\right.\right.$$

$$-\theta_{ab}^{\rho-}(\chi/2)]\Big)\Big\rangle_g$$

$$=\pm i\Big\langle \exp\Big(\pm i\frac{\sqrt{\pi}}{2}[\delta\phi_{ab}^{\rho-}(\chi/2)+\delta\phi_{ab}^{\rho-}(-\chi/2)$$

$$+\delta\theta_{ab}^{\rho-}(\chi/2)-\delta\theta_{ab}^{\rho-}(\chi/2)]\Big)\Big\rangle_g$$

$$=\pm i g_{ab}^{\rho-}(\Lambda\chi), \tag{4.40}$$

where $\chi=x/\Lambda\xi$, and we have without loss of generality chosen $X=0$, since the average is independent of X by translational invariance. The function $g_{ab}^{\rho-}(\chi)$ satisfies

$$0<g_{ab}^{\rho-}(0)\lesssim 1,\ g_{ab}^{\rho-}\sim C_1 e^{-C_2\chi},\quad \chi\gg 1, \tag{4.41}$$

with C_1 and C_2 order one constants. The exponential decay arises from the separation of the two $\theta_{ab}^{\rho-}$ fields, whose rapid fluctuations exponentially suppress the average. More formally, the correlator involves a ''string'' connecting $x=\pm\chi/2$, which carries an action per unit length (string tension) of $1/\xi$.

Similar reasoning leads to the results in the spin sector:

$$\Big\langle \exp\Big(\pm i\sqrt{\frac{\pi}{2}}[\phi_{d\sigma}(\chi/2)-\phi_{d\sigma}(-\chi/2)+\theta_{d\sigma}(\chi/2)$$

$$+\theta_{d\sigma}(\chi/2)]\Big)\Big\rangle_g=g_{d\sigma}(\Lambda\chi), \tag{4.42}$$

where $g_{d\sigma}(\chi)$ are functions with the same properties as $g_{ab}^{-\rho}$, Eq. (4.41).

The fourth factor emerging from the averages in Eq. (4.39) is the exponential of the $\phi_{ab}^{\rho+}$ field, which is not averaged over. At this point, therefore, the $\langle\hat{\Psi}_{d\pm}\rangle_g$ fields are still operators. Using Eqs. (4.40)–(4.42), they may be cast into the form

$$\langle\hat{\Psi}_{d\pm}(X,x)\rangle_g=\pm\Delta_d(x)e^{i\phi(X)}i\eta_{d\uparrow}\eta_{d\downarrow}, \tag{4.43}$$

where $\phi(X)=\sqrt{\pi}\phi_{ab}^{\rho+}(X/\Lambda\xi)$, and we have used the fact $x\lesssim\xi$ (enforced by $g_{ab}^{-\rho}$ and $g_{d\sigma}$) to neglect the x dependence of ϕ. The overall sign arises from reordering the Klein factors. Physically, we may now interpret ϕ as the usual $U(1)$ phase of the superconducting order parameter. The prefactor Δ_d is what is conventionally interpreted as the pair wave funcion in a superconductor, and has the form

$$\Delta_a(x)\equiv\frac{1}{2\pi\xi}g_{ab}^{\rho-}(x/\xi)g_{a\sigma}(x/\xi), \tag{4.44}$$

$$\Delta_b(x)\equiv-\frac{1}{2\pi\xi}g_{ab}^{\rho-}(x/\xi)g_{b\sigma}(x/\xi). \tag{4.45}$$

The relative minus sign between $\langle\hat{\Psi}_{d+}\rangle_g$, $\langle\hat{\Psi}_{d-}\rangle_g$ implies that the pair wave function is a spin singlet, as is demonstrated by rewriting this result as

$$\langle\hat{\Psi}_{Ri\alpha Lj\beta}(X,x)\rangle_g=\delta_{ij}\Delta_i(x)(\delta_{\alpha\uparrow}\delta_{\beta\downarrow}-\delta_{\alpha\downarrow}\delta_{\beta\uparrow})e^{i\phi(X)}. \tag{4.46}$$

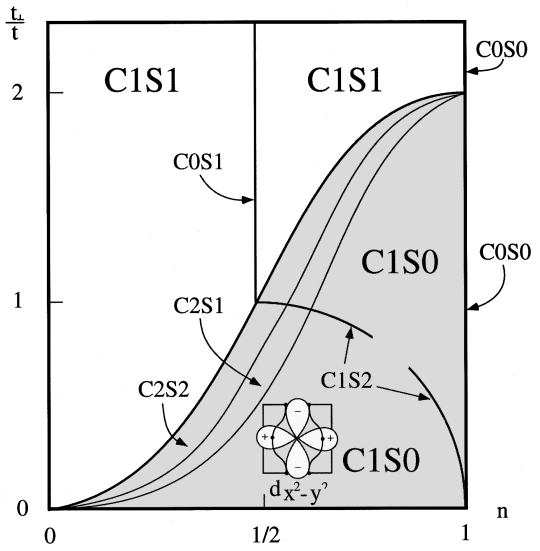

FIG. 6. Phase diagram of the two-chain Hubbard model with weak repulsive interactions.

As in conventional superconductors (SC), the ground state of the system is a singlet and, therefore, SU(2) invariant.

The relative sign between $\langle\hat{\Psi}_{a+}\rangle_g$, $\langle\hat{\Psi}_{b+}\rangle_g$ indicates that the pair wave function has d-wave symmetry in momentum space. This is illustrated in Figs. 6–10. The precise nature of the wave function, i.e., the distinction between $d_{x^2-y^2}$ and d_{xy} pairing, depends on the positions of (a,b) on the Fermi surface. To emphasize this point, we now calculate the pair wave function in real space.

The most general pairing operator in coordinate space is

$$\Psi(\mathbf{R},\mathbf{r},\alpha,\beta)=\psi_\alpha\Big(\mathbf{R}+\frac{\mathbf{r}}{2}\Big)\psi_\beta\Big(\mathbf{R}-\frac{\mathbf{r}}{2}\Big), \tag{4.47}$$

where $\mathbf{R}=(X,Y)$ is the coordinate of the center of mass, and $\mathbf{r}=(x,y)$ is the relative distance between the pairing electrons. Here α,β are the spin indices of the electron pair.

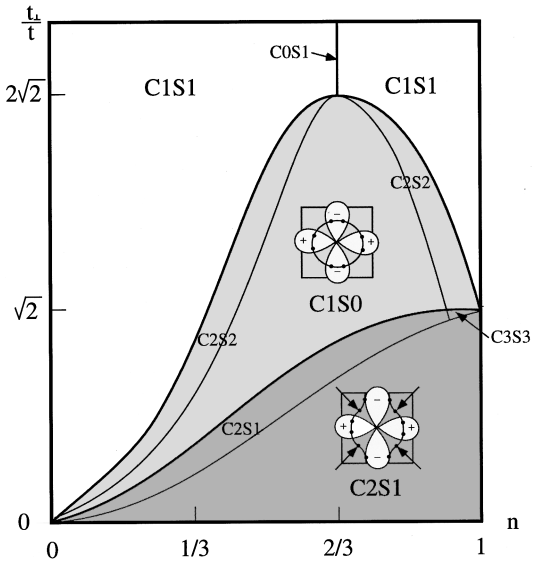

FIG. 7. Phase diagram of the three-chain Hubbard model for OBC's.

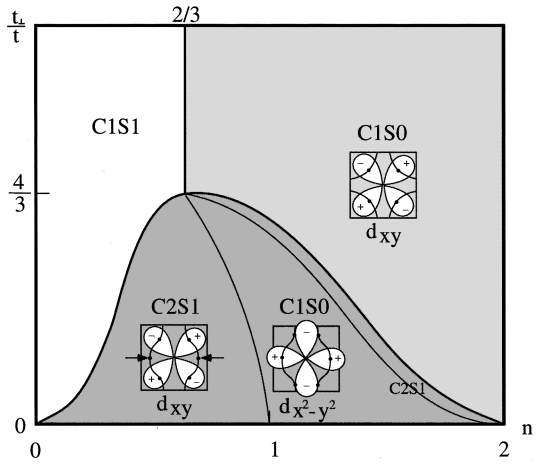

FIG. 8. Phase diagram of the three-chain Hubbard model for PBC's.

The pair fields $\hat{\Psi}$ [Eq. (4.32)] and Ψ [Eq. (4.47)] are essentially related by a Fourier transform in the transverse (P,i) indices. To make this explicit, we must keep track of boundary conditions. For OBC's, the right and left movers are standing waves in the transverse direction, and

$$\psi_\alpha(\mathbf{r}) \sim \{\psi_{Ri\alpha}(x)e^{ik_{Fi}x} + \psi_{Li\alpha}(x)e^{-ik_{Fi}x}\}\sin(k_{yi}y), \tag{4.48}$$

where k_{yi} are the transverse momenta defined in Eq. (2.8). For PBC's, because the system is translational invariant, the decomposition is the usual Fourier one,

$$\psi_\alpha(\mathbf{r}) \sim \psi_{Ri\alpha}(x)e^{i\mathbf{k}_{Fi}\mathbf{r}} + \psi_{Li\alpha}(x)e^{-i\mathbf{k}_{Fi}\mathbf{r}}, \tag{4.49}$$

where the Fermi vector $\mathbf{k}_{Fi} \equiv (k_{Fi}, 2\pi i/N)$.

Consider first OBC's. Using Eqs. (4.47) and (4.48),

$$\langle \Psi(\mathbf{R},\mathbf{r},\alpha,\beta)\rangle_g$$

$$\simeq \sum_{i,j} \{\sin(k_{yi}y_1)\sin(k_{yj}y_2)\psi_{i\alpha}(X+x/2)\psi_{j\beta}(X-x/2)\}$$

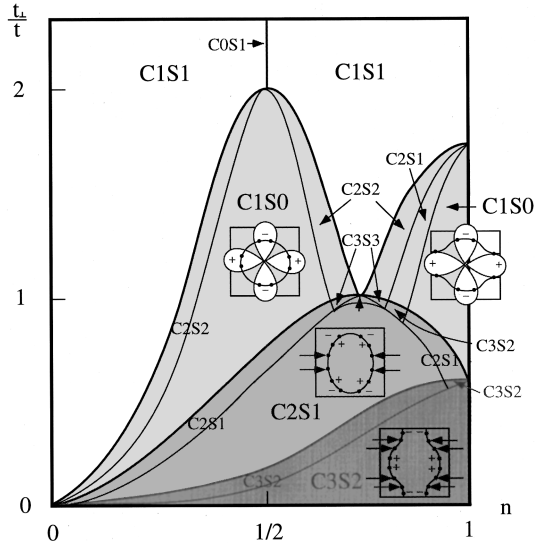

FIG. 9. Phase diagram of the four-chain Hubbard model for OBC's.

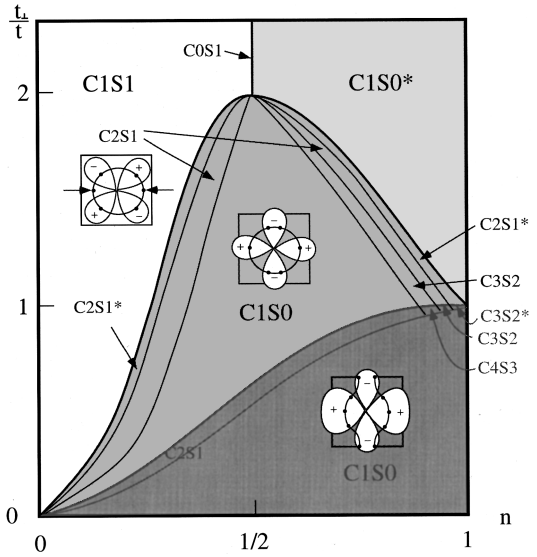

FIG. 10. Phase diagram of the four-chain Hubbard model for PBC's. The states marked with an asterisk exhibit CEX pairing.

$$\simeq \sum_{ij} \sin(k_{yi}y_1)\sin(k_{yj}y_2)$$
$$\times [\langle \hat{\Psi}_{Ri\alpha Lj\beta}(X,x)\rangle_g e^{ik_{Fi}(X+x/2)-ik_{Fj}(X-x/2)}$$
$$+ \langle \hat{\Psi}_{Li\alpha Rj\beta}(X,x)\rangle_g e^{-ik_{Fi}(X+x/2)+ik_{Fj}(X-x/2)}]. \tag{4.50}$$

In the second line, we have used the fact that the nonvanishing $\hat{\Psi}$ operators pair right and left moving fermions, and have thereby dropped $\hat{\Psi}_{RR}$ and $\hat{\Psi}_{LL}$ contributions. Using $\hat{\Psi}_{Li\alpha Rj\beta}(X,x) = -\hat{\Psi}_{Rj\beta Li\alpha}(X,-x)$, and $\Delta_i(-x) = \Delta_i(x)$ and Eq. (4.46), Eq. (4.50) leads to the familiar form

$$\langle \Psi(\mathbf{R},\mathbf{r},\alpha,\beta)\rangle_g = \Phi_d(Y,\mathbf{r})\chi_{\alpha\beta}e^{i\phi}. \tag{4.51}$$

The spatial and spin parts of the Cooper pair wave function are

$$\Phi_d^{\mathrm{OBC}}(Y,\mathbf{r}) = \sum_{i=a,b} 2\Delta_i(x)\cos(k_{Fi}x)\sin(k_{yi}y_1)\sin(k_{yi}y_2),$$

$$\chi_{\alpha\beta} = \delta_{\alpha\uparrow}\delta_{\beta\downarrow} - \delta_{\alpha\downarrow}\delta_{\beta\uparrow}. \tag{4.52}$$

The positions of the electrons are denoted as $y_{1,2} = [Y \pm (y/2)]$. Because of the hard-wall boundary conditions, the spatial part of wave function depends on the transverse center-of-mass coordinate Y. Because $\Delta_a\Delta_b < 0$, $\Phi_d^{\mathrm{OBC}}(\mathbf{r})$ has d-wave symmetry in real space.

For PBC's, the results are quite similar. The pairing operator retains the same form of Eq. (4.51), with instead

$$\Phi_d^{\mathrm{PBC}}(\mathbf{r}) = \sum_{i=a,b} 2\Delta_i(x)\cos(\mathbf{k}_{Fi}\mathbf{r}). \tag{4.53}$$

In this case, the wave function only depends on the relative coordinate $\mathbf{r}$ because the system is translational invariant. Once again, the symmetry is d-wave like.

D. Even chain PBC's

Turning to the case of even N with PBC's, the generic presence of transverse umklapp (u) interactions allows for a new RG instability. This possibility is realized for $N=4$, as we have found by numerically integrating the extended equations of Appendix B. In certain regions of the phase diagram, the Cooper (c) couplings become asymptotically irrelevant, and instead the transverse umklapp and forward-scattering interactions become dominant. As before, this occurs in only two bands, which we will again denote a and b. In order for these two bands to be connected by two-particle umklapp processes, they must satisfy $|a-b|=N/2$. More careful attention to the numerics shows that, in addition, these relevant couplings satisfy

$$u_{ab}^{1\rho}=\frac{1}{4}u_{ab}^{1\sigma}>0, \tag{4.54}$$

$$f_{a\bar{a}}^{\sigma}<0, f_{b\bar{b}}^{\sigma}<0. \tag{4.55}$$

Equations (4.54) and (4.55) appear quite similar to Eqs. (4.20) and (4.21), already encountered in the generic case. In fact, careful study shows that the instability encountered here is mathematically equivalent, after a relabeling of the bands, to the earlier case. Instead of repeating the analysis of the previous subsection *ad infinitum*, we will therefore instead only sketch the essential points of the parallel treatment needed here.

To account for the change in paired bands, we combine the chiral boson modes into the modified canonically conjugate fields,

$$\overline{\theta_{i\alpha}}=\phi_{Ri\alpha}-\phi_{L\bar{i}\alpha},$$
$$\overline{\phi_{i\alpha}}=\phi_{Ri\alpha}+\phi_{L\bar{i}\alpha}. \tag{4.56}$$

Defining spin and charge bosons as in Eq. (4.14), the interaction terms become

$$\mathcal{H}_{\rm int}^{(1)}+\mathcal{H}_{\rm int}^{(2)}\sim\sum_{i=a,b} f_{i\bar{i}}^{\sigma}\cos(\sqrt{8\pi}\overline{\theta_{i\sigma}}) + 4u_{ab}^{1\sigma}\cos(\sqrt{4\pi}\overline{\phi_{ab}^{\rho-}})\sin(\sqrt{2\pi}\overline{\theta_{a\sigma}}) \times\sin(\sqrt{2\pi}\overline{\theta_{b\sigma}}), \tag{4.57}$$

where $\overline{\phi_{ab}^{\rho\pm}}\equiv(\overline{\phi_a^{\rho}}\pm\overline{\phi_b^{\rho}})/\sqrt{2}$. This is of the same form as Eq. (4.19) and the semiclassical analysis is identical, with $\theta\leftrightarrow\theta$ and $\phi\leftrightarrow\phi$. All the subsequent steps of the analysis carry through with small modifications. The nonvanishing partially averaged pair fields expressed in terms of band indices are

$$\langle\hat{\Psi}_{Ri\alpha Lj\beta}\rangle_g=\delta_{i\bar{j}}\overline{\Delta_i}(x)\chi_{\alpha\beta}e^{i\phi(X)}, \tag{4.58}$$

where $\phi(X)=\sqrt{\pi}\overline{\phi_{ab}^{\rho+}}(X/\Lambda\xi)$, and the gap functions in momentum space are

$$\overline{\Delta_a}=\frac{\Lambda}{2\pi\xi}\,\overline{g_{ab}^{\rho-}}(x/\xi)\overline{g_{a\sigma}}(x/\xi),$$
$$\overline{\Delta_b}=-\frac{\Lambda}{2\pi\xi}\,\overline{g_{ab}^{\rho-}}(x/\xi)\overline{g_{b\sigma}}(x/\xi). \tag{4.59}$$

Notice that electrons with opposite k_x but the *same* k_y are paired. This implies that the Cooper pair carries nonzero transverse *quasimomentum*. To clarify the situation further, we now specialize to the case of primary interest, $N=4$. Following the previous subsection, we can again put the pairing operator into real space. Equation (4.51) continues to hold, but with

$$\overline{\Phi}_{N=4}(Y,x)=\sum_{i=a,b}2\overline{\Delta_i}(x)\cos(k_{Fi}x)e^{i2k_{yi}Y} =-4|\overline{\Delta_a}|(x)\cos(k_{Fa}x)\sin(\pi Y), \tag{4.60}$$

where we have used reflection symmetry which implies $\overline{g_{a\sigma}}=\overline{g_{b\sigma}}$ in Eq. (4.59), and hence $\overline{\Delta_a}=-\overline{\Delta_b}$, as well as $k_{Fa}=k_{Fb}=\pi/2$ in this case. Note that Y takes on integer and half-integer values, so that Φ is real but can vary in sign. If one imagines wrapping the four chains around into a cylinder, the Y dependence is simply a superposition of the $m=\pm2$ angular momentum states, i.e.,

$$\sin(\pi Y)=\sin(2\Theta), \tag{4.61}$$

where $\Theta=\pi Y/2$ is the angle around the cylinder. For this reason, we call this a CEX d-wave state. Note that since the superposition here is purely real, the state does not carry any spontaneous current.

V. PHASE DIAGRAMS

In the previous sections, we have described the RG and bosonization technology necessary to analyze a weakly interacting one-dimensional Fermi system for any generic set of parameter values. We have, of course, applied these methods to study the particularly interesting case of the N-chain Hubbard models. The detailed calculations involve lengthy but straightforward numerical integrations of the RG equations and mapping out the ensuing pairing instabilities as a function of N, n, and $t_\perp/t$. The primary *results* of this work are the phase diagrams shown in Figs. 6–10. For the most part these stand on their own, but we will comment on a few points.

A. Commonalities

1. Band transitions

In the weak-coupling limit, it is natural that the gross features of the phase diagrams are dictated by the noninteracting band structure. In particular, the $n-t_\perp/t$ plane is divided into distinct regions, in each of which a particular number N_f of 1D bands are *partially* filled (and hence not inert). The boundaries between these regions constitute band transitions, which generally survive as phase boundaries in the weakly interacting system.

While the band transitions need not be the only phase boundaries in the interacting system, they usually form the most noticable divisions of the phase space. To locate them, one must solve Eqs. (2.7), (2.8), (2.10), (2.11) for the lines along which $\epsilon_a(0)=\mu$ (band a is just empty) or $\epsilon_a(\pi)=\mu$ (band a is just full), for each a. These curves are indicated in the figures by heavy lines. The shading of the regions separated by the heavy lines indicates the number N_f of partially

filled bands, with white corresponding to $N_f=1$ and the darkest shade corresponding to $N_f=N$.

2. Band-edge phases

On one side of such a band transition, the ''critical'' band (let us denote its index by $a=E$) is almost empty or almost filled. This gives rise to a very small Fermi velocity, $v_E \ll t$, in the weak-coupling RG. For such a small velocity, the dimensionless couplings acting purely within the band E are greatly enhanced: $g_{EE}=\tilde{g}_{EE}/(2\pi v_E) \gg g_{aE}$, for $a \neq E$. Physically, this increased scattering is due simply to the large density of states near the 1D van Hove singularity at the edge of the band.

Strictly speaking, the RG equations as we have derived them are not valid directly at the band transition. This is because the spectrum of an empty/full band is not relativistic but quadratic ($\omega \sim k^2/2m$), demanding a different (anisotropic) scaling. We can, however, approach very close to the band transition in the weak-coupling limit. That is, provided that we keep $U/v_E \ll 1$ (a much more stringent requirement than $U/t \ll 1$), Eqs. (3.7)–(3.10) remain valid.

In this region, the nearly vanishing Fermi velocity provides a useful small parameter. Indeed, those couplings within band E are (at least initially) much larger than those involving any of the noncritical bands. For the initial stages of integration of the RG flows, then, these ''edge-band'' interactions dominate the evolution of the couplings. In particular, they lead to a decoupling of the critical band from the remaining degrees of freedom. To see this, consider the evolution of the interactions between band E and another band i. In the Cooper channel,

$$\begin{pmatrix} \dot{c}^{\rho}_{iE} \\ \dot{c}^{\sigma}_{iE} \end{pmatrix} \approx -\begin{pmatrix} c^{\rho}_{EE} & \frac{3}{16}c^{\sigma}_{EE} \\ c^{\sigma}_{EE} & c^{\rho}_{EE}+\frac{1}{2}c^{\sigma}_{EE} \end{pmatrix} \begin{pmatrix} c^{\rho}_{iE} \\ c^{\sigma}_{iE} \end{pmatrix}. \tag{5.1}$$

Because the initial value for the Hubbard model,

$$\begin{pmatrix} c^{\rho}_{iE}(0) \\ c^{\sigma}_{iE}(0) \end{pmatrix} = \begin{pmatrix} 1 \\ 4 \end{pmatrix} c^{\rho}_{iE}(0), \tag{5.2}$$

happens to be one of the eigenvectors of the matrix in Eq. (5.1), the solution is particularly simple:

$$c^{\sigma}_{iE}(l)=4c^{\sigma}_{iE}(l) \simeq C_1 e^{-(C_2/v_E)l}, \tag{5.3}$$

where C_1, C_2 are constants of $O(U)$.

This exponential decay holds provided the *running* couplings within band E ($c^{\rho}_{EE}, c^{\sigma}_{EE}$) remain large compared to the interband couplings. Examination of Eqs. (3.9) and (3.10) shows that the intra-edge-band couplings relax logarithmically to zero in the initial flow regime. The above equations are thus valid for

$$c^{\rho}_{EE}, c^{\sigma}_{EE} \sim \frac{1}{l} \gg c^{\rho}_{kE}, \quad c^{\sigma}_{kE} \sim \frac{U}{v_k}. \tag{5.4}$$

Following Eq. (5.3) out to this, we see that the couplings to the critical band are indeed exponentially suppressed

$$c^{\sigma}_{iE}(l=v_k/U)=4c^{\sigma}_{iE}(l=v_k/U) \simeq \tilde{C}_1 \exp[-\tilde{C}_2 v_k/v_E], \tag{5.5}$$

where $\tilde{C}_1$ and $\tilde{C}_2$ are order one constants.

To complete the argument that band E becomes decoupled from the others, we must now show that this suppression persists into the regime of divergence of other couplings, i.e., to the cutoff scale l^*. To do so, we employ the algebraic relations valid in the asymptotic regime [Eq. (4.8)]. Consider, for example, the relation derived from Eq. (3.9). The contributions on the right-hand side can be separated into singular and nonsingular parts,

$$C^{\sigma}_{kl} = -\alpha_{kl,E} C^{\sigma}_{kE} C^{\sigma}_{lE} + (\text{nonsingular terms}), \tag{5.6}$$

where $k,l \neq E$. Here we have used the relaton $C^{\sigma}_{ij}=4C^{\rho}_{ij}$ as usual. Since the factor $\alpha_{kl,E} \sim 1/v_E$ is singular when $v_E \to 0$, there are only two possible options. Either the singularity in $\alpha_{kl,E}$ is cancelled, and $C_{kE} \sim \sqrt{v_E}$, or the singular and nonsingular parts equal zero separately and

$$C^{\sigma}_{kE}=0. \tag{5.7}$$

The former possibility is inconsistent with the exponential suppression in Eq. (5.5), so we expect that instead Eq. (5.7) holds and the couplings c_{kE} will flow to zero in the asymptotic regime. This is indeed observed in all numerical integrations of the full RG equations near a band transition.

This decoupling implies that the low-energy structure of the system is obtained by adding the single gapless charge and spin modes of the critical band to the low-energy structure of the remaining bands that would have occurred were band E inert. To determine the phase of the Hubbard model in the band-edge regime, therefore, we may simply add $C1S1$ to the gapless mode content on the other side of the band transition, in which the critical band is indeed inert. If the phase on this side is $C_N S_M$, then the band-edge result on the other side of the transition line is

$$C_N S_M + C1S1 = C_{N+1} S_{M+1}. \tag{5.8}$$

B. Specific features

1. ''d-wave'' pairing

Probably the most striking aspect of the phase diagrams is the ubiquity of paired states—i.e., gapping out of the spin modes in at least some of the bands. Following the methods of Sec. IV, these pairing instabilities can be associated with a gap function defined at the allowed discrete points on the 2D Fermi surface. Except in certain regions of phase space in the four-chain model, this gap function has an approximate ''d-wave'' form. For $N \geq 3$, a d-wave gap has an interesting consequence in this context: the discrete transverse wave vectors k_{ya} can coincide with the nodes in the pair wave function. This indeed occurs, e.g., near half-filling for $N=3$ with OBC's for $t_\perp < \sqrt{2}t$, giving rise to simultaneous dominant superconducting correlations and power-law antiferromagnetism. The d-wave interpretation begins to break down, however, for $N=4$ with OBC's, where several gapless spin modes are present for small $t_\perp/t$. The unusual distribution of gapped and ungapped modes on the Fermi surface in this case is, we expect, a consequence of the one-dimensional

weak-coupling limit taken here, which becomes rather restrictive for larger N. A more complete discussion of the approach to a two-dimensional weak-coupling limit is described in Sec. VI.

2. Peculiarities of PBC's

The systems with PBC's exhibit a number of (theoretically) interesting peculiarities. For $N=3$, some of these have been pointed out by Arrigoni,[30,31] who performed a similar weak-coupling analysis. For odd N, the effects of PBC's can be expected to be rather severe. In the Hubbard model, they break particle-hole symmetry, which has the effect of eliminating reflection symmetry of the phase diagram around half filling. Furthermore, half filling no longer coincides with the conditions needed for umklapp processes at the Fermi level. This has the happy consequence that our generic treatment (which ignores these umklapp interactions) remains valid at $n=1$. One then finds the rather surprising result that the half-filled system has gapless charge excitations and a spin gap, precisely the opposite of what is expected in the strong-coupling limit with OBC's, where there is a charge gap ($\sim U$), and the effective Heisenberg model (with odd N) is expected to have a gapless spin mode. Some partial understanding can be gained from the fact that an odd-chain Heisenberg model with PBC's is *frustrated*, and can be shown (at least for $N=3$) to indeed have a spin gap. However, the absence of a charge gap is a weak-coupling result, and indicates the existence of a *metal-insulator transition* at half filling as U is increased. Interestingly, the weak-coupling paired state can be either of d_{xy} or $d_{x^2-y^2}$ type, as indicated in Fig. 8.

A different sort of feature arises for PBC's with $N=4$. Although this situation retains particle-hole symmetry, there nevertheless exist regions (the largest occurs for weak doping with $t_\perp > t$) in which the finite transverse size has a severe effect. This CEX d-wave phase has a pair wave function whose phase depends upon the *transverse center-of-mass coordinate* of the pair. This phenomenon is described in Sec. IV D, and is certainly special to the one-dimensional cylindrical geometry considered here.

3. Extreme asymptotic instability of the C1S0 phase

A number of authors have predicted the existence of a $C1S0$ paired state for a weakly interacting two-chain Hubbard ladder. As noted (in proof) in Ref. 13 in the asymptotic limit $U/t \to 0^+$, the $C1S0$ phase in fact occurs only for infinitesimal doping, being replaced everywhere else by the $C2S1$ phase. For reasonable (but still small) values in the range $10^{-6} < U/t \lesssim 1$, however, the $C1S0$ phase still appears as dominant.

To understand this result requires a more detailed examination of the asymptotic regime near the RG divergence. To do so, we again consider the algebraic relations described in Sec. IV A.

Using Eq. (4.8), we look for a solution of the resulting algebraic equations for which $C_{12}^\sigma \neq 0$, corresponding to a $C1S0$ phase. Some straightforward calculations give the unique answer

$$C_{11}^\sigma = C_{22}^\sigma = -\frac{1}{2}(1+\sqrt{1-4\alpha_{11,2}C_{12}^\sigma}), \tag{5.9}$$

$$1+\frac{3}{2}C_{11}^\sigma - \frac{1}{2}(1+\alpha_{11,2})C_{12}^\sigma = 0. \tag{5.10}$$

Now consider the stability of this solution. From Eq. (3.10), the difference between c_{11}^σ and c_{22}^σ obeys

$$\frac{d}{dl}(c_{11}^\sigma - c_{22}^\sigma) = -(c_{11}^\sigma - c_{22}^\sigma)(c_{11}^\sigma + c_{22}^\sigma). \tag{5.11}$$

Since c_{ii}^σ are negative near the divergent point l^*, the difference of Cooper couplings $c_{11}^\sigma - c_{22}^\sigma$ is relevant, and the above solution is in fact *unstable*. For the special initial value $c_{11}^\sigma - c_{22}^\sigma = 0$, which is attained in the limit $n \to 1$, the system is specially tuned to an unstable equilibrium, and the $C1S0$ phase enjoys a small region of existence. Moving away from half filling, however, the inequality of Fermi velocities in bands 1 and 2 destroys this fine-tuning, driving the system away from the $C1S0$ state. In the asymptotic limit, the stable solution is in fact the much simpler $C2S1$ flow. This point has been missed in other calculations, owing to the assumption of equal Fermi velocities[14,26] and the lack of a careful stability analysis of the asymptotic regimes.[11,30,31] We emphasize, however, that numerically this instability is extremely weak. For even relatively weak couplings with $10^{-6} < U/t \lesssim 1$, we find that the $C1S0$ phase remains quasistable, occupying in fact the majority of the two-chain phase diagram.

VI. DIMENSIONAL CROSSOVER

In this section, we discuss how the system approaches 2D behavior as $N \to \infty$. The limit is actually quite subtle, and we will consider two distinct ways of performing it. The simplest procedure is simply to attempt to preserve the validity of the RG as presented here [Eqs. (3.7)–(3.10)]. This $1d$ *weak-coupling limit* can be realized in principle for any fixed (but large) N for sufficiently small U, but taking $N \to \infty$ actually requires that the interactions vanish as well. A more physically appealing approach is the true $2D$ *weak-coupling limit*, in which $N \to \infty$ for a fixed (but small) U. In this case, the RG as constructed so far must in principle be supplemented by additional interactions.

A. One-dimensional weak-coupling limit

We first consider the naive limit of the RG flows [Eqs. (3.7)–(3.10)] as $N \to \infty$. Recalling the results of Sec. II [Eq. (2.46)], to retain the validity of these equations, the interactions must be simultaneously taken to zero, with $U \lesssim t/\ln N$. Since this constraint is only logarithmic in N, this is actually not a strong restriction even for reasonably large values of N, and might indeed be physically relevant in some systems.

In the large N limit, the RG flows are dominated by those terms involving sums over intermediate band indices; which effectively increase these terms by a factor of N. To make the largest terms of order one for large N, we introduce the rescaled coupling constants

$$c_{ij}^\rho = \frac{1}{N}\frac{2\sqrt{v_i v_j}}{v_i + v_j}\hat{c}_{ij}^\rho, \tag{6.1}$$

and similarly for the other interaction channels. Note that, with Hubbard initial conditions, the values of $\hat{c}^{\rho}_{ij}$ are of an order of one (in N). Inserting this into Eqs. (3.7)–(3.10) and dropping the $O(1/N)$ terms, one finds that the forward and umklapp scattering vertices are exactly marginal (unrenormalized). The Cooper channel interactions obey the simplified equations

$$\partial_l \hat{c}^{\rho}_{ij} = -\frac{1}{N}\sum_k \left(\hat{c}^{\rho}_{ik}\hat{c}^{\rho}_{kj} + \tfrac{3}{16}\hat{c}^{\sigma}_{ik}\hat{c}^{\sigma}_{kj}\right), \tag{6.2}$$

$$\partial_l \hat{c}^{\sigma}_{ij} = -\frac{1}{N}\sum_k \left(\hat{c}^{\rho}_{ik}\hat{c}^{\sigma}_{kj} + \hat{c}^{\sigma}_{ik}\hat{c}^{\rho}_{kj} + \tfrac{1}{2}\hat{c}^{\sigma}_{ik}\hat{c}^{\sigma}_{kj}\right). \tag{6.3}$$

The Hubbard model initial condition that $4c^{\rho}_{ij}(0) = c^{\sigma}_{ij}(0)$ is preserved by Eq. (6.3), so they may be collapsed into the single nontrivial RG equation,

$$\frac{d\hat{c}^{\sigma}_{ij}}{dl} = -\frac{1}{N}\sum_k \hat{c}^{\sigma}_{ik}\hat{c}^{\sigma}_{kj}. \tag{6.4}$$

Note that the right-hand side of Eq. (6.4) has the form of matrix multiplication. This implies that, provided the initial couplings matrix is diagonalizable, each eigenvalue λ_i of the matrix c^{σ} evolves independently according to

$$\frac{d\lambda_i}{dl} = -\frac{1}{N}\lambda_i^2. \tag{6.5}$$

Focusing for simplicity on PBC's, the initial value of $\hat{c}^{\sigma}$ is

$$\hat{c}^{\sigma}_{ij}(0) = \left(\frac{U}{2\pi}\right)\frac{1}{\sqrt{v_i v_j}}. \tag{6.6}$$

Since this has the form of an outer product, it is proportional to a projection operator onto the vector $1/\sqrt{v_i}$. It thus has $N_f - 1$ null vectors and a single nontrivial eigenvector proportional to $1/\sqrt{v_i}$.[41,42] The eigenvalues are

$$\lambda_i(0) = \left(\frac{U}{2\pi}\sum_k \frac{1}{v_k}\right), 0, \ldots, 0. \tag{6.7}$$

From Eq. (6.5), the N_f zero eigenvalues are unchanged under the RG, while λ_1 obeys

$$\lambda_1(l) = \frac{N\lambda_1(0)}{N + \lambda_1(0)l}, \tag{6.8}$$

where $\lambda_1(0) = (U/2\pi)\Sigma_k 1/v_k$. Since $\lambda_1(0) > 0$, it is marginally irrelevant and flows to zero. This implies that all the Cooper interactions flow logarithmically to zero.

To connect with previous two-dimensional treatments, we may define a simple continuum limit:

$$\hat{c}^{\sigma}_{ij} \to V(k_{yi}, k_{yj}), \tag{6.9}$$

$$\frac{1}{N}\sum_i \to \int_{-\pi}^{\pi}\frac{dk_{yi}}{2\pi}, \tag{6.10}$$

which gives the RG equation

$$\frac{d}{dl}V(k_y, k_y') = -\int_{-\pi}^{\pi}\frac{dk_y''}{2\pi}V(k_y, k_y'')V(k_y'', k_y'), \tag{6.11}$$

as derived previously by Shankar[33] directly in 2D.

B. Two-dimensional weak-coupling limit

On reflection, the agreement with approaches directly in two dimensions is perhaps surprising, since the RG equations used above are valid only for $U/t \lesssim 1/\ln N$ as $N \to \infty$. To study the true 2D weak-coupling limit (with $U/t \ll 1$ but fixed as $N \to \infty$) requires consideration of the additional shifted interactions (such as $\mathcal{H}^s$) introduced in Sec. II C. Fortunately, one can show that, even upon including these interactions, the modifications of the RG equations are actually negligible in weak coupling. Rather than belabor this reasoning, which is essentially discussed already in, e.g., Shankar's review article,[33] we will only schematically indicate how this comes about.

Once the additional shifted interactions are included in the RG, we must worry about two questions. How do these new vertices renormalize, and how do they feed back into the flow equations for the unshifted couplings? In answer to the first question, under normal conditions, the shifted interactions renormalize almost identically to their unshifted counterparts, at least in the initial stages of the RG. This is because for each process involving two unshifted vertices feeding into an unshifted vertex, there is an analogous process involving the same vertices shifted, usually feeding back into the analogous shifted vertex. Next, note that, in weak coupling, the range of momentum shifts is highly constrained:

$$|\Delta k_y| = 2\pi|\delta|/N < 2\pi\delta_{\max}/N \sim \Lambda t_\perp/t,$$

$$\Rightarrow |\Delta k_y| \lesssim |\Delta k_y|_{\max} = \pi\frac{t_\perp}{t}e^{-\text{const } t/U}, \tag{6.12}$$

as can be seen from Eqs. (2.44) and (2.15). For any nonsingular interaction, the initial coupling constants are reasonably smooth in momentum space, so that all the shifted interactions in the narrow range $|k_{y\delta}| < |\Delta k_y|$ are essentially equal in magnitude. Since each shifted vertex then has the same initial conditions and obeys the same RG equation as an unshifted coupling, it remains so under the RG, and the original equations remain sufficient to study their evolution.

It remains to answer the second question. There *are* a few additional processes involving the shifted interactions, such as the one shown in Fig. 11, which feed back into the original Cooper- and forward-scattering channels. The feedback into the forward-scattering channel is negligible for the same phase-space reasons that render them exactly marginal for $N \to \infty$ above. More subtle is the feedback into the unshifted Cooper channel. Once shifted vertices are included, an intermediate sum over δ allows for nonvanishing contributions of the form

$$\frac{d\hat{c}^{\sigma}_{ij}}{dl} = \cdots + \frac{\text{const}}{N}\sum_{\delta}\hat{c}^{\sigma}_{i(j-\delta)}(\delta)\hat{f}^{\sigma}_{i(j-\delta)}(\delta) + \cdots, \tag{6.13}$$

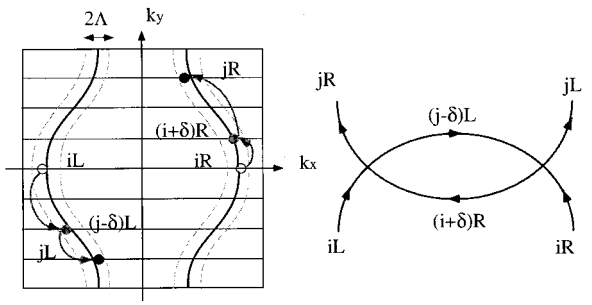

FIG. 11. An example of renormalization of c_{ij}^{σ} from shifted vertices in Eq. (6.13).

in which the (shifted) forward-scattering vertices feed back into the Cooper channel even as $N\to\infty$ (since $\delta_{\max}/N$ is finite in this limit). However, the phase space for these renormalizations is considerably smaller than the processes already included. Roughly speaking, these additional terms are down by a factor of $\Lambda/\pi\sim\exp(-\text{const}\times t/U)$ from the others, since the range of angles of the intermediate momenta are restricted to a width $|\Delta k_y|_{\max}\ll 2\pi$. Furthermore, the number of allowed terms continues to decrease as the RG proceeds to lower energies, since the band curvature $t_\perp/t$ effectively grows under rescaling.

C. Instabilities for $1\ll N\ll\infty$

In the large N limit, therefore, additional (shifted) interactions *are* present at weak but finite couplings, but do not modify the RG equations or their analysis as presented above. At $N=\infty$, then, the 2D metal is marginally stable.[41] What occurs in weak coupling for large but finite N? Our numerical results suggest that instabilities always persist when feedback of forward-scattering interactions into the Cooper channel is included. However, this cross coupling is an $O(1/N)$ effect, and so is extremely weak for large N. Specifically, these terms can only begin to affect the flows once the Cooper interactions have themselves renormalized down to order $1/N$. Since the $N=\infty$ flows are logarithmic, this occurs only after a rescaling $b=e^{l}\sim e^{N}$, so that the characteristic energy gaps (and critical temperatures) of any paired states should obey

$$\Delta_N\lesssim e^{-N}, \tag{6.14}$$

with a prefactor which is not determinable by such coarse arguments.

This exponential decrease of the energy scale for pairing is a signature of the rather robust stability of the generic Fermi liquid. This weak-coupling result, however, does not make any statement about pairing instabilities for *strong* repulsive interactions. Nongeneric situations can, of course, give rise to much larger energy scales, even at weak coupling. Of particular importance in highly anisotropic repulsively interacting systems is the spin-density-wave instability. Because this requires nesting in weak coupling, the associated interaction vertices have been thrown out in our calculations.

VII. DISCUSSION

The principal results of this paper are the N-chain weak-coupling phase diagrams, described in detail for small and large N in Secs. V and VI, respectively. We now conclude with a discussion of the *implications* of these results for both ideal finite N systems (accessible via numerical calculations) and for true quasi-one-dimensional systems, where nonzero interladder couplings need to be taken into account.

A. Numerics

Numerical calculations have the advantage that direct comparisons with 1D models can be made. Recall that each phase is characterized at the simplest level by its number of gapless charge and spin modes. These numbers can be measured numerically in a number of ways. Most directly, the lowest-lying charge and spin excitation energies can be determining by comparing ground state energies (in, e.g., exact diagonalization or density-matrix RG methods) with particles added or spins flipped. Such measurements can also be refined to determine the energies for the lowest-lying excitations with a definite *parity*, which can be related to the band indices used here. The *total number* of gapless modes (both charge and spin) can in principle be extracted alternatively from the coefficient of $1/L$ (where L is the chain length) in the finite-size correction to the ground-state energy density.

The parity of the ground state and low-lying excited states are also accessible in weak coupling. Here we focus on the $C1S0$ phase in a two-chain system as an example. The parity operator of a two-chain system is

$$P=\exp(i\pi N_2), \tag{7.1}$$

where N_2 is the total number of particles in the antibonding band. The parity operator P commutes with the Hamiltonian, so that parity is a good quantum number. If the ground state is a linear superposition of states with odd/even N_2, it has odd/even parity. In the $C1S0$ phase, if total number of particles is even, N_2 is even because electrons pair up in both bands. Therefore, the ground state has even parity. However, if the total number is odd, the analysis is complicated and remains an open question for further study. The parities of excited states is determined by commutation relation between the corresponding creation operators and parity operator. The Bosonic field operator $\phi_{12}^{\rho+}(p)$, which is the only gapless mode in the $C1S0$ phase, creates a density excitation with momenta p. If we express N_2 in terms of the bosonic fields

$$N_2=\sqrt{2\pi}\{\theta_{2\rho}(\infty)-\theta_{2\rho}(-\infty)\}, \tag{7.2}$$

it is easy to show that $\phi_{12}^{\rho+}(p)$ commutes with the parity operator. This implies that the excited state has the same parity as the ground state. In other words, the excitation carries even parity. Consequently, numerical calculations should find a *charge gap* in the odd-parity channel, despite the exsistence of a gapless charge mode with even parity. A simple test is the correlation function

$$C(x)=\langle\Delta\rho(x)\Delta\rho(0)\rangle, \tag{7.3}$$

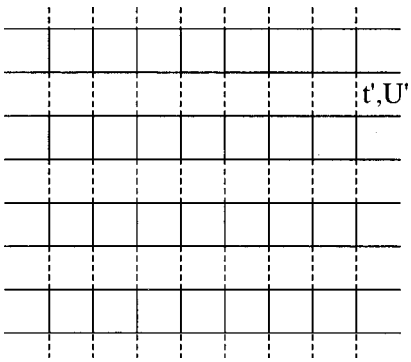

FIG. 12. A 2D array of Hubbard ladders, with weak interladder hopping t' and interladder density-density interaction U'.

where $\Delta\rho(x) \equiv c_{1\alpha}^{\dagger} c_{1\alpha}(x) - c_{2\alpha}^{\dagger} c_{2\alpha}(x)$. Since $P^{\dagger}\Delta\rho P = -\Delta\rho$, $C(x)$ has only odd-parity (relative to the ground state) intermediate states, and should therefore decay *exponentially*, $C(x) \sim e^{-\Delta\rho - x/v}$.

It is often more convenient to compute correlation functions rather than ground state energies (indeed, in a Monte Carlo calculation, this is essentially the only option). In this case, the information that can be most reliably assayed is the presence or absence of charge and spin gaps. If there is a true gap in either sector, the corresponding correlators are expected to decay exponentially in space. To probe the charge sector, the correlators of interest are those of the density $\rho = c_{\alpha}^{\dagger} c_{\alpha}$ and the pair field $\Delta = c_{\uparrow} c_{\downarrow}$. In the spin sector, the corresponding operator is simply the spin $\mathbf{S} = c_{\alpha}^{\dagger} (\sigma/2)\, c_{\beta}$. In principle, a detailed examination of the Fourier content of the correlations should identify the Fermi momenta of the gapless spin and charge modes (even more information than their number), but this is quite difficult in practice due to finite-size limitations imposed by the numerics.

B. Experimental consequences

Comparison with experiments is more challenging. In particular, it is inevitably the case that in any candidate compound there is at least some residual coupling between ladders as shown in Fig. 12. In this sense, all real materials are at best quasi-one-dimensional. It is to the features of such quasi-one-dimensional ladder materials and the regime of validity of the previous results in this context to which we now turn. The discussion will be kept at a general level, using only scaling considerations. We take as a model a two- or three-dimensional regular array of N-chain ladders, the precise geometry of which is not crucial, although special cases resulting in Fermi-surface nesting will not be addressed. A microscopic electronic model for such an array would involve the hopping amplitudes and interactions both on and between the ladders. We will assume that the former are of the Hubbard form studied in the previous sections. The latter generically introduce two new energy scales: an interladder hopping amplitude t' and an interladder density-density interaction U' (Fig. 12). For now, we assume that *at least* $t'/t, U'/t \ll 1$.

1. Weak interactions

To proceed, let us imagine repeating the weak-coupling RG with these additional interactions. Upon first integrating out the large wave vector modes ($|k_x| > \Lambda$) on each ladder, t' and U' will suffer small renormalizations, and other new interactions will also be generated. Two of these are of particular importance: two-particle hopping processes, in which two Fermions are simultaneously transferred from one ladder to a neighbor, and four-particle ''pair-density'' interactions, in which fermions interact energetically on neighboring ladders in a manner quartic in the density, but no charge is transferred. These will occur with a pair-hopping amplitude t'' and a pair-density interaction U'', which are approximately

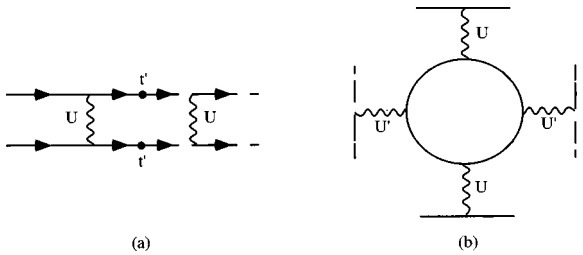

FIG. 13. Lowest-order diagrams illustrating the generation of interchain pair-hopping t'' and pair-density interactions U'' from the bare interchain hopping t' and density interaction U'.

$$t'' \sim (t')^2 U^2 / t^3, \tag{7.4}$$

$$U'' \sim (U')^2 U^2 / t^3, \tag{7.5}$$

in the weak-coupling limit (see Fig. 13). For generality, we shall keep t'' and U'' as independent parameters. Other interactions are of course also generated, but are either of similar type but much smaller magnitude than those already considered, or are higher-order and hence at least perturbatively irrelevant.

At this point, we proceed with the RG as before, working perturbatively in t'/t, t''/t, U'/t, and U''/t. Like the original ladder parameters, these will also rescale and nonlinearly renormalize themselves and other couplings. The corrections to Eqs. (3.7)–(3.10) will, however, be negligible provided the values of the *running* couplings $t'/t|_l, t''/t|_l, U'/t|_l, U''/t|_l \lesssim g_i(l)$. Initially, this of course requires $t', t'', U', U'' \ll U$, but the constraints become stronger as we iterate to lower-energy scales. In particular, for the divergences encountered purely within the ladder RG to be essentially unchanged requires that the running interladder couplings be negligible compared to one (since the relevant ladder couplings become of order one) at the scale $l^* \sim ct/U$, where c is a constant. Simple power counting gives

$$\frac{\partial}{\partial l}\left(\frac{t'}{t}\right) \approx \frac{t'}{t}, \tag{7.6}$$

$$\frac{\partial}{\partial l}\left(\frac{t''}{t}\right) \approx \left(\frac{t''}{t}\right)^2, \tag{7.7}$$

$$\frac{\partial}{\partial l}\left(\frac{U'}{t}\right) \approx \left(\frac{U'}{t}\right)^2, \tag{7.8}$$

$$\frac{\partial}{\partial l}\left(\frac{U''}{t}\right)\approx -2\frac{U''}{t}, \tag{7.9}$$

since t', t'', U', and U'' represent two-, four-, four-, and eight-fermion operators. The hopping t'/t thus grows exponentially, the two-particle processes $t''/t, U'/t$ scale only logarithmically (are marginal), and the pair-density interaction U'' is strongly irrelevant. The 1D RG results are then valid up to the instability scale l^* provided

$$t' \lesssim t e^{-ct/U} \sim \Delta, \tag{7.10}$$

$$t'' \lesssim U, \tag{7.11}$$

$$U' \lesssim U, \tag{7.12}$$

$$U'' \lesssim t e^{2ct/U} \sim t^3/\Delta^2, \tag{7.13}$$

where Δ is the energy scale of the gap in the 1D system [note that factors of (t/U) in the prefactor are not captured within a one-loop RG treatment, so this is a rough estimate and not a strict asymptotic statement]. The requirement of $t' \lesssim \Delta$ has a simple physical interpretation: for $t' \gtrsim \Delta$, it is favorable for singlet pairs to break up to reduce their kinetic energy, destroying the paired state.

Provided Eqs. (7.10)–(7.13) are satisfied, the strong-coupling analysis of Sec. IV holds, and the paired bands are adequately described by the single collective phase mode $\phi^{\rho+}$ (and its conjugate $\theta^{\rho+}$). For concreteness, we now specialize to the two-chain case, where there are no additional bands. The single-particle tunneling operator conjugate to t' then involves exponentials of the dual fields $\phi_{a\sigma}$ [c.f. Eq. (4.28)], which fluctuate wildly and are exponentially suppressed (strongly irrelevant). Similarly, the density-density interaction U' is also negligible due to strong fluctuations of the relative-displacement mode $\theta^{\rho-}$. The remaining two couplings (t'' and U'') survive, and have simple interpretations. The pair-hopping, t'' simply hops a single boson between neighboring ladders, and is hence like a Josephson coupling. The pair-density coupling U'' is effectively a density-density interaction between bosons on neighboring ladders, which are created by the pair fields of Sec. IV. In terms of the phases, the effective Hamiltonian is

$$H_{\rm eff} = \int dx \Bigg\{ \sum_n \left[\frac{Kv}{2}(\partial_x \phi_n^{\rho+})^2 + \frac{v}{2K}(\partial_x \theta_n^{\rho+})^2 \right] - \sum_{\langle nn' \rangle} \Bigg[t'' \cos\sqrt{\pi}(\phi_n^{\rho+} - \phi_{n'}^{\rho+}) + \frac{U''}{\xi^2}\cos 2\sqrt{\pi}(\theta_n^{\rho+} - \theta_{n'}^{\rho+}) \Bigg] \Bigg\}, \tag{7.14}$$

where the index n labels the different ladders, and we have taken the cutoff scale $\Lambda = 1$ for simplicity. The factor of ξ^{-2} in the pair-density interaction reflects its irrelevance at the noninteracting fermion fixed point, and results directly from integration of Eq. (7.9). As discussed in Ref. 13 the stiffness K is not exactly determinable within the weak-coupling RG for generic parameters. However, various arguments suggest $K > 1/2$,[43] and, in particular, $K \approx 1$ close to half filling in the two-leg ($N=2$) ladder[14] at weak coupling.

To determine the nature of the ground state of the system, we must now address the physics at energy scales below Δ. To do this, we use a different RG rescaling, using standard sine-Gordon techniques.[44] This gives the linear flow equations,

$$\frac{\partial}{\partial l} t'' \approx \left(2 - \frac{1}{2K}\right) t'' + O[(t'')^2, (U'')^2], \tag{7.15}$$

$$\frac{\partial}{\partial l} U'' \approx (2-2K) U'' + O[(t'')^2, (U'')^2]. \tag{7.16}$$

Note that the Josephson coupling t'' is relevant for $K > 1/4$, while the pair-density interactions are relevant for $K < 1$. There is therefore no region of stability for truly one-dimensional behavior, regardless of K. Most probably $1/2 < K < 1$, and *both* perturbations are relevant. If both the dimensionless bare interactions are weak, $t''/t, U''/(t\xi^2) \ll 1$, then the nature of the instability is determined by the interaction which renormalizes to large (order one) values first. Simple algebra thus predicts that pair-tunneling dominates for

$$\left(\frac{t''}{t}\right)^{2-2K} \gtrsim \left(\frac{U''}{t\xi^2}\right)^{2-1/(2K)}, \tag{7.17}$$

and the ladders phase lock into a bulk SC state. In the opposite limit, pair-density interactions dominate and lead to a paired-insulator or charge-density wave (CDW) state. Note that for K close to 1, the SC state dominates for all but extremely small t''. Generically, though, as t'' is reduced below the limit of Eq. (7.17), the system makes a transition to the CDW state.

Let us now use the estimates in Eqs. (7.4) and (7.5) to determine the bulk phase diagram for the two-chain system in the weak-coupling limit. As t' is decreased, the pairing instability occurs first, according to Eq. (7.10), when $t' \lesssim \Delta$. Just below this scale, it is straightforward to show that this instability always leads to a SC rather than CDW, provided $U/t \ll 1$, as supposed. This is because Eq. (7.17) can be rewritten, using Eqs. (7.4) and (7.5) and the scaling of the dimensionless coherence length $\xi \sim t/\Delta$, as

$$\frac{t'}{t} \gtrsim \frac{t}{U}\left[\frac{U'U\Delta}{t^3}\right]^{(1-1/4K)/(1-K)}, \tag{7.18}$$

and $[1-1/(4K)]/(1-K) \geqslant 1$ for $K > 1/2$. Only for much smaller t' does this inequality cease to hold and the system go over into a CDW state. A schematic zero-temperature phase diagram for fixed small U/t with these features is shown in Fig. 14.

Supposing the system is in the SC phase at zero temperature, what is the expected phenomenology as the temperature is varied? In weak coupling, we expect several large crossover ranges. For $T \gg T_{\rm pair} \sim \Delta$, the system acts approximately in a noninteracting 1D fashion, with small logarithmic corrections which are precursors of the instability to be encountered for $T \simeq T_{\rm pair}$. Below that temperature scale pairing effectively occurs, and measurements (e.g., magnetic susceptibility or electron tunneling) probing single-particle and spin excitations should exhibit activated behavior. How-

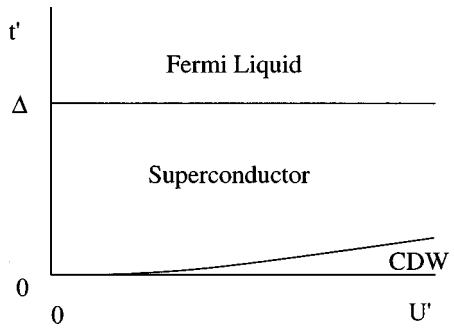

FIG. 14. Schematic zero-temperature phase diagram in the t'-U' plane for an array of coupled ladders.

ever, although pairs form at $T_{\rm pair}$, superconducting coherence sets in only at a lower temperature, $T_{\rm sc}$.

To see this, we continue rescaling after reaching l^*, i.e., to energies below the spin gap. We can now rescale further, as indicated above, until the rescaled temperature grows to the order of the energy cutoff, at which point the zero-temperature RG fails. Having already rescaled to $l^* \sim \ln(t/\Delta)$, the effective temperature has already been increased to $(t/\Delta)T$, but for $T \lesssim \Delta$, this is still small relative to the cutoff t, and we can rescale further by the factor $b \sim \Delta/T$. At this point the temperature is on the order of the cutoff, and thermal smearing is sufficient to remove any remaining quantum coherence at lower energies. The corresponding length $L_{\rm qc} \sim v/T$ represents a quantum to classical crossover scale at temperature T. Fluctuations of larger size behave essentially classically (as can be shown explicitly by restricting the rescaled effective action to the zero Matsubara frequency modes) and can be studied using the rescaled classical (phase only) model

$$\beta H_{\rm class} = \int dx \Bigg\{ \sum_n \frac{K}{2} (\partial_x \phi_n^{\rho+})^2 - \sum_{\langle nn' \rangle} \frac{t''}{t} \left(\frac{\Delta}{T} \right)^{2-1/2K} \cos \sqrt{\pi} (\phi_n^{\rho+} - \phi_{n'}^{\rho+}) \Bigg\}. \tag{7.19}$$

This classical model has only a single dimensionless coupling constant, as can be seen by rescaling $x \to x/K$. The superconducting transition must occur when this dimensionless value is order one, giving the critical temperature

$$T_{\rm sc} \sim \Delta \left(\frac{t''}{t} \right)^{2K/(4K-1)}, \tag{7.20}$$

valid within the SC region of the phase diagram away from the zero-temperature quantum SC-CDW transition. Note that for $t'' \ll t$, there is a large temperature range $T_{\rm sc} \ll T \ll T_{\rm pair}$ over which the system has a ''pseudo-gap-like'' behavior. The difference between the exponent $2K/(4K-1)$ and 1/2 (the classical result for weakly coupled 1D XY chains) represents a suppression of the transition temperature due to quantum fluctuations.

2. Beyond weak interactions

Although the analysis of this paper has assumed $U \ll t$, many two-chain models have now been convincingly demonstrated, numerically and in some limits analytically, to display spin gaps when weakly doped even for relatively strong interactions (e.g., $U \gtrsim t$). In fact, most aspects of the phenomenology in this conclusion are expected to continue to hold even in this limit, provided that the *interchain* couplings are small, $U', t' \ll t$. In particular, on physical grounds, we expect a transition to a Fermi liquid (or at least two-dimensional behavior) for $t' \gtrsim \Delta$. For $t' \lesssim \Delta$, interchain couplings essentially never break pairs, and the physics will still be well-described by Eq. (7.14) at these and lower-energy scales. Of course, in strong coupling the parameters t'' and U'' cannot be estimated using the weak-coupling diagrams of Fig. 13 leading to Eqs. (7.4) and (7.5). In addition, it is difficult in strong coupling to determine K: recent numerical simulations with $U/t = 8$ suggest values of $K \approx 1/2$,[43] somewhat smaller (and hence less superconducting) than in weak coupling. With these caveats, the remaining phenomenology should continue to hold, both for the zero-temperature phase diagram and for the crossovers and transitions at $T > 0$.

ACKNOWLEDGMENTS

We are grateful to Doug Scalapino for illuminating conversations. This work has been supported by the National Science Foundation under Grant Nos. PHY94-07194, DMR-9400142, and DMR-9528578.

APPENDIX A: CURRENT ALGEBRA

Current-algebra methods allow, among other things, an *algebraic* calculation of the one-loop RG equations. Here we give a very terse description of this method. All currents are defined in terms of the fermion fields $\psi_{R/Li\alpha}$ $(i = 1,2,\ldots,N)$, which obey the operator products,

$$\psi_{Ri\alpha}(x,\tau)\psi^\dagger_{Rj\beta}(0,0) \sim \frac{\delta_{ij}\delta_{\alpha\beta}}{2\pi z_i} + O(1),$$

$$\psi_{Li\alpha}(x,\tau)\psi^\dagger_{Lj\beta}(0,0) \sim \frac{\delta_{ij}\delta_{\alpha\beta}}{2\pi z_i^*} + O(1), \tag{A1}$$

where $z_i = v_i\tau - ix$. The operator products should be understood to hold when two points (x,τ) and (0,0) are brought close together. We therefore only need to keep the singular terms as replacement within correlation functions. As an example, consider the product $J_{ij}J_{lm}$. Performing all possible contractions gives

$$\begin{aligned} J_{ij}(x,\tau)J_{lm}(0,0) &\sim :\psi^\dagger_{i\alpha}\psi_{j\alpha}::\psi^\dagger_{l\beta}\psi_{m\beta}: \\ &\sim \frac{2}{4\pi^2 z_i z_j}\delta_{im}\delta_{jl} + \frac{\delta_{im}}{2\pi z_i}:\psi_{j\alpha}\psi^\dagger_{l\alpha}: \\ &\quad + \frac{\delta_{jl}}{2\pi z_j}:\psi^\dagger_{i\alpha}\psi_{m\alpha}: + :J_{ij}J_{lm}: \\ &\sim \left(\frac{\delta_{jl}}{2\pi z_j} J_{im} - \frac{\delta_{im}}{2\pi z_i} J_{lj} \right) + \delta_{im}\delta_{jl}\frac{2}{4\pi^2 z_i z_j} \end{aligned}$$

$$+O(1). \tag{A2}$$

We can compute the full set of operator products in a similar way. The ones needed are

$$J^a_{ij}J^b_{lm}\sim \frac{1/2}{4\pi^2 z_i z_j}\delta_{im}\delta_{jl}+\frac{\delta_{ab}}{4}\left(\frac{\delta_{jl}}{2\pi z_j}J_{im}-\frac{\delta_{im}}{2\pi z_i}J_{lj}\right)+\frac{i\epsilon^{abc}}{2}\left(\frac{\delta_{jl}}{2\pi z_j}J^c_{im}+\frac{\delta_{im}}{2\pi z_i}J^c_{lj}\right), \tag{A3}$$

$$J^a_{ij}J_{lm}\sim \frac{\delta_{jl}}{2\pi z_j}J^a_{im}-\frac{\delta_{im}}{2\pi z_i}J^a_{lj}, \tag{A4}$$

where the coordinates of two operators on each left-hand side are consecutively (x,τ) and (0,0). Similar forms hold for the left-moving currents, but with $z_i\rightarrow z_i^*$.

The RG equations can be obtained very simply from the operator product expansions. We use the functional integral formulation which results in the Euclidean action, $S_E=\int dx\ d\tau\mathcal{H}$, and the partition function,

$$\mathcal{Z}=\int [d\overline{\psi}][d\psi]e^{-S_E}. \tag{A5}$$

To perform the RG, the exponential is expanded to quadratic order in $\mathcal{H}$. A typical term takes the form,

$$\frac{1}{2}\widetilde{f}^{\sigma}_{ij}\widetilde{f}^{\sigma}_{lm}\int_{z,w}\langle J^a_{Rii}(z)J^a_{Ljj}(z)J^b_{Rll}(w)J^b_{Lmm}(w)\rangle, \tag{A6}$$

where $\int_{z,w}$ denotes a four-dimensional integral over the two complex planes z and w. As in any RG, we wish to integrate out the short-scale degrees of freedom to derive the effective theory at long wavelengths and low energy. Here this is accomplished by considering the contributions to Eq. (A6) when the two points z and w are close together (near the cutoff scale). We make use of the operator product expansion to integrate out the short-scale degrees of freedom, which gives

$$\frac{1}{2}(\widetilde{f}^{\sigma}_{ij})^2 i\epsilon^{abc}i\epsilon^{abd}\int_{z,w}\frac{1}{2\pi(z_i-w_i)}\frac{1}{2\pi(z_j^*-w_j^*)}J^c_{Rii}J^d_{Ljj}. \tag{A7}$$

We choose a short distance cutoff $a=\Lambda^{-1}$ in space, but none in imaginary time. For a rescaling factor b, we must then perform the integral,

$$I_{ij}=\int_{a<|x|<ba}dx\int_{-\infty}^{\infty}d\tau\frac{1}{(2\pi)^2 z_i z_j^*}=\frac{\ln b}{\pi(v_i+v_j)}, \tag{A8}$$

where z is the relative coordinates in Eq. (A8). The contribution to the RG equation after integration is

$$-\frac{(\widetilde{f}^{\sigma}_{ij})^2}{\pi(v_i+v_j)}dl\int_z \mathbf{J}_{Rii}\mathbf{J}_{Ljj}, \tag{A9}$$

where $dl=\ln b$ is the logarithmic length scale. This term, when reexponentiated, renormalizes $\widetilde{f}^{\sigma}_{ij}$ and gives the first term in Eq. (3.8). All other terms in the RG equations can be carried out by similar steps.

APPENDIX B: RG EQUATIONS OF UMKLAPP INTERACTIONS

For PBC's, when the number of chains is even, we need to study the transverse umklapp interactions in addition to the forward and Cooper vertices. We then obtain additional terms on the right-hand sides of Eqs. (3.7)–(3.10). Denoting these by $\delta f_{ij},\delta c_{ij}$, one finds

$$\delta\dot{f}^{\rho}_{ij}=-\delta_{i\bar{J}}\sum_k \alpha_{ii,k}\{(u^{1\rho}_{ik})^2+\tfrac{3}{16}(u^{1\sigma}_{ik})^2\}-\{(u^{2\rho}_{ij})^2+\tfrac{3}{16}(u^{2\sigma}_{ij})^2\}+\sum_a\{(u^{a\rho}_{i\bar{J}})^2+\tfrac{3}{16}(u^{a\sigma}_{i\bar{J}})^2\}, \tag{B1}$$

$$\delta\dot{f}^{\sigma}_{ij}=-\delta_{i\bar{J}}\sum_k \alpha_{ii,k}\{2u^{1\rho}_{ik}u^{1\sigma}_{ik}+\tfrac{1}{2}(u^{1\sigma}_{ik})^2\}-\{2u^{2\rho}_{ij}u^{2\sigma}_{ij}+\tfrac{1}{2}(u^{2\sigma}_{ij})^2\}+\sum_a\{2u^{a\rho}_{i\bar{J}}u^{a\sigma}_{i\bar{J}}-\tfrac{1}{2}(u^{a\sigma}_{i\bar{J}})^2\}, \tag{B2}$$

$$\delta\dot{c}^{\rho}_{ij}=\delta_{ij}\{(u^{1\rho}_{i\bar{\imath}})^2+\tfrac{3}{16}(u^{1\sigma}_{i\bar{\imath}})^2\}+2(u^{1\rho}_{i\bar{J}}u^{2\rho}_{i\bar{J}}+\tfrac{3}{16}u^{1\sigma}_{i\bar{J}}u^{2\sigma}_{i\bar{J}}), \tag{B3}$$

$$\delta\dot{c}^{\sigma}_{ij}=\delta_{ij}\{2u^{1\rho}_{i\bar{\imath}}u^{1\sigma}_{i\bar{\imath}}-\tfrac{1}{2}(u^{1\sigma}_{i\bar{\imath}})^2\}+2(u^{2\rho}_{i\bar{J}}u^{1\sigma}_{iJ}+u^{1\rho}_{iJ}u^{2\sigma}_{i\bar{J}}-\tfrac{1}{2}u^{1\sigma}_{iJ}u^{2\sigma}_{i\bar{J}}). \tag{B4}$$

We also need the RG equations for the umklapp couplings themselves, which are

$$\dot{u}^{1\rho}_{ij}=(q^{\rho}_{ij}u^{1\rho}_{ij}+\tfrac{3}{16}q^{\sigma}_{ij}u^{1\sigma}_{ij})+2(c^{\rho}_{i\bar{J}}u^{2\rho}_{ij}+\tfrac{3}{16}c^{\sigma}_{i\bar{J}}u^{2\sigma}_{ij}), \tag{B5}$$

$$\dot{u}^{1\sigma}_{ij}=(q^{\rho}_{ij}u^{1\sigma}_{ij}+q^{\sigma}_{ij}u^{1\rho}_{ij}-\tfrac{1}{2}q^{\sigma}_{ij}u^{1\sigma}_{ij})-(f^{\sigma}_{i\bar{\imath}}+f^{\sigma}_{j\bar{J}})u^{1\sigma}_{ij}+2(c^{\rho}_{i\bar{J}}u^{2\sigma}_{ij}+c^{\sigma}_{i\bar{J}}u^{2\rho}_{ij}-\tfrac{1}{2}c^{\sigma}_{i\bar{J}}u^{2\sigma}_{ij}), \tag{B6}$$

$$\dot{u}^{2\rho}_{ij}=2(c^{\rho}_{i\bar{J}}u^{1\rho}_{ij}+\tfrac{3}{16}c^{\sigma}_{i\bar{J}}u^{1\sigma}_{ij})+2(p^{\rho}_{ij}u^{2\rho}_{ij}+\tfrac{3}{16}p^{\sigma}_{ij}u^{2\sigma}_{ij}), \tag{B7}$$

$$\dot{u}^{2\sigma}_{ij}=2(c^{\rho}_{i\bar{J}}u^{1\sigma}_{ij}+c^{\sigma}_{i\bar{J}}u^{1\rho}_{ij}-\tfrac{1}{2}c^{\sigma}_{i\bar{J}}u^{1\sigma}_{ij})+2(p^{\rho}_{ij}u^{2\sigma}_{ij}+p^{\sigma}_{ij}u^{2\rho}_{ij}-\tfrac{1}{2}p^{\sigma}_{ij}u^{2\sigma}_{ij})-2f^{\sigma}_{ij}u^{2\sigma}_{ij}, \tag{B8}$$

where $p^{\alpha}_{ij}\equiv f^{\alpha}_{i\bar{J}}-f^{\alpha}_{ij}$ and $q^{\alpha}_{ij}\equiv 2\delta_{i\bar{J}}c^{\alpha}_{ii}+(2f^{\alpha}_{i\bar{J}}-f^{\alpha}_{i\bar{\imath}}-f^{\alpha}_{j\bar{J}})$, $\alpha=\rho,\sigma$.

APPENDIX C: INITIAL VALUES OF THE COUPLINGS

Upon changing to the band basis, the on-site Hubbard repulsion is transformed into a set of interactions between the different bands. Using Eq. (2.3), we have

$$-\mathcal{H}_{\rm int}=-U\sum_i :c^{\dagger}_{i\uparrow}(x)c_{i\uparrow}(x)c^{\dagger}_{i\downarrow}(x)c_{i\downarrow}(x): \tag{C1}$$

$$= -U\sum_{ijkl} A_{ijkl} :\psi^\dagger_{i\uparrow}\psi_{j\uparrow}\psi^\dagger_{k\downarrow}\psi_{l\downarrow}:,$$

$$\text{where } A_{ijkl}\equiv\sum_m S^*_{mi}S_{mj}S^*_{mk}S_{ml}. \tag{C2}$$

Consider first OBC's. After linearizing around the Fermi points, each operator is split into left and right moving pieces. In terms of these,

$$-\mathcal{H}_{\rm int} = -U\sum_{ijkl}\sum_{P_i=\pm} A_{ijkl} :\psi^\dagger_{P_1 i\uparrow}\psi_{P_2 j\uparrow} \times\psi^\dagger_{P_3 k\downarrow}\psi_{P_4 l\downarrow}: e^{i(-P_1k_{F1}+P_2k_{F2}-P_3k_{F3}+P_4k_{F4})}. \tag{C3}$$

Now we are ready to compare the coefficients of interactions in Eqs. (2.29), (C3). For example, comparing the coefficient in front of the term $\psi^\dagger_{Ri\uparrow}\psi_{Ri\downarrow}\psi^\dagger_{Li\downarrow}\psi_{Li\uparrow}$ yields the relation

$$\frac{1}{2}\widetilde{f}^\sigma_{ij} = UA_{ijji} = UA_{iijj}. \tag{C4}$$

Comparing the coefficients of $\psi^\dagger_{Ri\uparrow}\psi_{Ri\uparrow}\psi^\dagger_{Li\downarrow}\psi_{Li\downarrow}$ gives

$$-(\hat{f}^\rho_{ij}+\tfrac{1}{4}\widetilde{f}^\sigma_{ij}) = -UA_{iijj}. \tag{C5}$$

We can then solve for the initial values of the forward couplings.

$$\widetilde{f}^\sigma_{ij} = 4\widetilde{f}^\rho_{ij} = 2UB_{ij},$$

$$\text{where } B_{ij}\equiv\sum_m |S_{mi}|^2|S_{mj}|^2. \tag{C6}$$

A straightforward computation gives

$$B_{ij} = \frac{1}{N+1}\left(1+\frac{1}{2}\delta_{i+j,N+1}+\frac{1}{2}\delta_{i,j}\right). \tag{C7}$$

By similar comparisons, we obtain the initial values of the Cooper couplings,

$$\widetilde{c}^\sigma_{ij} = 4\widetilde{c}^\rho_{ij} = 2UA_{ijij} = 2UB_{ij}, \tag{C8}$$

where in the last step we use the fact that the transformation matrix S_{ij} in Eq. (2.5) is real for OBC's.

For PBC's, similar results can be obtained by this method. Taking care to note the different conventions for left and right movers for PBC's [see Eq. (2.17)], the initial values of the forward and Cooper couplings are

$$\widetilde{f}^\sigma_{ij} = 4\widetilde{f}^\rho_{ij} = 2UA_{ii\overline{JJ}}, \tag{C9}$$

$$\widetilde{c}^\sigma_{ij} = 4\widetilde{c}^\rho_{ij} = 2UA_{ij\overline{\imath J}}, \tag{C10}$$

where $\overline{\imath} = -i$. From Eq. (2.4), one can compute these initial values. These are

$$\widetilde{f}^\sigma_{ij} = 4\widetilde{f}^\rho_{ij} = \frac{2U}{N}, \tag{C11}$$

$$\widetilde{c}^\sigma_{ij} = 4\widetilde{c}^\rho_{ij} = \frac{2U}{N}. \tag{C12}$$

If the number of chains is even, we also need the initial values of the transverse umklapp couplings. In fact, the initial values are the same as those for the forward and Cooper couplings:

$$\widetilde{u}^{1\sigma}_{ij} = 4\widetilde{u}^{1\rho}_{ij} = \frac{2U}{N}, \tag{C13}$$

$$\widetilde{u}^{2\sigma}_{ij} = 4\widetilde{u}^{2\rho}_{ij} = \frac{2U}{N}. \tag{C14}$$

Note that, in all case, the initial values of the rescaled couplings in Eqs. (3.7)–(3.10) (without the tildes) are obtained by multiplying the factor $1/\pi(v_i+v_j)$.

APPENDIX D: REPRESENTATIONS FOR THE KLEIN FACTORS

The Klein factors defined in Eq. (4.9) satisfy the commutation relations,

$$\{\eta_{i\alpha},\eta_{j\beta}\} = 2\delta_{ij}\delta_{\alpha\beta}. \tag{D1}$$

In order to bosonize the relevant interactions in Eq. (4.18), we need to prove that the products of the Klein factors in different terms commute with each other. Then, they can be simultaneously diagonalized with a specific choice of representation.

The products of the Klein factors for the first term in Eq. (4.18) are

$$\eta_{d\uparrow}\eta_{d\downarrow}\eta_{d\downarrow}\eta_{d\uparrow} = \eta_{d\downarrow}\eta_{d\uparrow}\eta_{d\uparrow}\eta_{d\downarrow} = 1. \tag{D2}$$

For the second term, the Klein factors we need are

$$\eta_{a\uparrow}\eta_{a\downarrow}\eta_{b\downarrow}\eta_{b\uparrow} = \eta_{a\downarrow}\eta_{a\uparrow}\eta_{b\uparrow}\eta_{b\downarrow} \equiv g. \tag{D3}$$

A simple computation gives $g^2=1$. Thus, all the products of Klein factors in the above equations commute with each other. It is therefore consistent to choose the trivial representation $g=1$. For the cases of interest, then, no special signs or auxiliary fermion fields are necessary in the bosonized Hamiltonian.

[1] H. J. Schulz, Phys. Rev. B **34**, 6372 (1986).

[2] E. Dagotto, J. Riera, and D. Scalapino, Phys. Rev. B **45**, 5744 (1992).

[3] T. M. Rice, S. Gopalan, and M. Sigrist, Europhys. Lett. **23**, 445 (1993).

[4] I. Affleck, Rev. Math. Phys. **6**, 887 (1994).

[5] S. White, R. Noack, and D. Scalapino, Phys. Rev. Lett. **73**, 886 (1994).

[6] M. Azuma *et al.*, Phys. Rev. Lett. **73**, 3463 (1994).

[7] D. Tennant *et al.*, Phys. Rev. B **52**, 13 381 (1995).

[8] A. Keren *et al.*, Phys. Rev. B **48**, 12 926 (1993).

[9] S. Satija *et al.*, Phys. Rev. B **21**, 2001 (1980).

[10] A. Finkel'stein and A. Larkin, Phys. Rev. B **47**, 10 461 (1993).
[11] M. Fabrizio, Phys. Rev. B **48**, 15 838 (1993).
[12] K. Kuroki and H. Aoki, Phys. Rev. Lett. **72**, 2947 (1994).
[13] L. Balents and M. P. A. Fisher, Phys. Rev. B **53**, 12 133 (1996).
[14] H. J. Schulz, Phys. Rev. B **53**, R2 959 (1996).
[15] N. Nagaosa, Solid State Commun. **94**, 495 (1995).
[16] E. Orignac and T. Giamarchi, Phys. Rev. B **53**, R10 453 (1996).
[17] S. Kivelson, D. Rokhsar, and J. Sethna, Phys. Rev. B **35**, 8865 (1987).
[18] P. Anderson, Science **235**, 1196 (1987).
[19] R. Noack, S. White, and D. Scalapino, Phys. Rev. Lett. **73**, 882 (1994).
[20] R. Noack, S. White, and D. Scalapino, Europhys. Lett. **30**, 163 (1995).
[21] E. Dagotto and T. Rice, Science **271**, 618 (1996).
[22] C. Hayward *et al.*, Phys. Rev. Lett. **75**, 926 (1995).
[23] C. Hayward and D. Poilblanc, Phys. Rev. B **53**, 11 721 (1996).
[24] K. Sano, J. Phys. Soc. Jpn. **65**, 1146 (1996).
[25] M. Troyer, H. Tsunetsugu, and T. Rice, Phys. Rev. B **53**, 251 (1996).
[26] H. J. Schulz, cond-mat/9605075 (unpublished).
[27] T. Kimura, K. Kuroki, and H. Aoki, Phys. Rev. B **54**, R9 608 (1996).
[28] T. Kimura, K. Kuroki, and H. Aoki, J. Phys. Soc. Jpn. **66**, 1599 (1997).
[29] K. Penc, H. Shiba, F. Mila, and T. Tsukagoshi, Phys. Rev. B **54**, 4056 (1996).
[30] E. Arrigoni, Phys. Status Solidi B **195**, 425 (1996).
[31] E. Arrigoni, Phys. Lett. A **215**, 91 (1996).
[32] D. J. Scalapino (private communication).
[33] R. Shankar, Rev. Mod. Phys. **66**, 129 (1994).
[34] J. Negele and H. Orland, in *Quantum Many-Particle Systems* (Addison-Wesley, Redwood City, California, 1988), Chap. 2.
[35] C. Varma and A. Zawadowski, Phys. Rev. B **32**, 7399 (1985).
[36] K. Penc and J. Solyom, Phys. Rev. B **41**, 704 (1990).
[37] A. Ludwig, in *Quantum Field Theory and Condensed Matter Physics*, edited by S. Randjbar-Daemi and Y. Lu (World Scientific, Singapore, 94).
[38] J. Cardy, in *Phase Transitions and Critical Phenomena*, edited by C. Domb and J. Lebowitz (Academic Press, London, 1987).
[39] R. Shankar, Acta Phys. Pol. B **26**, 1835 (1995).
[40] V. Emery, in *Highly Conducting One-Dimensional Solids*, edited by J. Devreese, R. Evrard, and V. Van Doren (Plenum Press, New York, 1979), p. 247.
[41] The one-step integration gives $O(U^2)$ corrections to $c_{ij}^{\sigma}(0)$ which could induce negative eigenvalues in some of the N_f-1 directions whose bare eigenvectors vanish. This mechanism can lead to extremely weak superconducting instabilities (the Kohn-Luttinger effect) even in weak coupling, as discussed in this context by Zanchi and Schulz (Ref. 42).
[42] D. Zanchi and H. J. Schulz, Phys. Rev. B **54**, 9509 (1996).
[43] R. Noack, N. Bulut, D. Scalapino, and M. Zacher, cond-mat/9612165 (unpublished).
[44] J. Jose, L. Kadanoff, S. Kirkpatrick, and D. Nelson, Phys. Rev. B **16**, 1217 (1977).